

MM FILE COPY

4

AFGL-TR-87-0300

ENVIRONMENTAL RESEARCH PAPERS, NO. 988

Balloon-Borne, High-Altitude Gravimetry The Flight of DUCKY II (October 1985)

ANDREW LAZAREWICZ
BRENDA SCHILINSKI, MAJOR, USAF
LEONARD CARTER, LT COL, USAF
RALPH COWIE
CARL LEYH

AD-A202 985



28 October 1987



Approved for public release; distribution unlimited.



DTIC
ELECTE
DEC 16 1988
S E D



EARTH SCIENCES DIVISION

PROJECT 7600

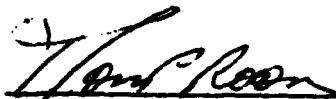
AIR FORCE GEOPHYSICS LABORATORY

HANSCOM AFB, MA 01731

88 12 16 038

"This technical report has been reviewed and is approved for publication"

FOR THE COMMANDER


THOMAS P. ROONEY, Chief
Geodesy & Gravity Branch


DONALD H. ECKHARDT
Director
Earth Sciences Division

This document has been reviewed by the ESD Public Affairs Office (PA) and is releasable to the National Technical Information Service (NTIS).

Qualified requestors may obtain additional copies from the Defense Technical Information Center. All others should apply to the National Technical Information Service.

If your address has changed, or if you wish to be removed from the mailing list, or if the addressee is no longer employed by your organization, please notify AFGL/DAA, Hanscom AFB, MA 01731. This will assist us in maintaining a current mailing list.

Do not return copies of this report unless contractual obligations or notices on a specific document requires that it be returned.

REPORT DOCUMENTATION PAGE				Form Approved OMB No. 0704-0188	
1a. REPORT SECURITY CLASSIFICATION Unclassified			1b. RESTRICTIVE MARKINGS N/A		
2a. SECURITY CLASSIFICATION AUTHORITY			3. DISTRIBUTION/AVAILABILITY OF REPORT Approved for public release; distribution unlimited.		
2b. DECLASSIFICATION/DOWNGRADING SCHEDULE					
4. PERFORMING ORGANIZATION REPORT NUMBER(S) AFGL-TR-87-0309 ERP, No. 988			5. MONITORING ORGANIZATION REPORT NUMBER(S)		
6a. NAME OF PERFORMING ORGANIZATION Air Force Geophysics Laboratory		6b. OFFICE SYMBOL (If applicable) AFGL/LWG	7a. NAME OF MONITORING ORGANIZATION		
6c. ADDRESS (City, State, and ZIP Code) Hanscom AFB Massachusetts 01731			7b. ADDRESS (City, State, and ZIP Code)		
8a. NAME OF FUNDING/SPONSORING ORGANIZATION		8b. OFFICE SYMBOL (If applicable)	9. PROCUREMENT INSTRUMENT IDENTIFICATION NUMBER		
8c. ADDRESS (City, State, and ZIP Code)			10. SOURCE OF FUNDING NUMBERS		
PROGRAM ELEMENT NO. 62101F		PROJECT NO. 7600	TASK NO. 06	WORK UNIT ACCESSION NO. 10	
11. TITLE (Include Security Classification) Balloon-Borne, High-Altitude Gravimetry The Flight of DUCKY II (October 1985)					
12. PERSONAL AUTHOR(S) Andrew Lazarewicz; Brenda Schilinski, Major, USAF; Leonard Carter, Lt Col, USAF*; Ralph Cowie, and Carl Levh					
13a. TYPE OF REPORT Scientific. Final.		13b. TIME COVERED FROM 9/83 TO 9/87	14. DATE OF REPORT (Year, Month, Day) 1987 October 28		15. PAGE COUNT 66
16. SUPPLEMENTARY NOTATION *Air Force Reserves					
17. COSATI CODES			18. SUBJECT TERMS (Continue on reverse if necessary and identify by block number)		
FIELD	GROUP	SUB-GROUP	Balloon High-altitude		
			Gravity		
			Gravimetry. (cdc) ←		
19. ABSTRACT (Continue on reverse if necessary and identify by block number)					
<p>→ Gravity measurements from a high-altitude balloon were made in October 1985 to verify global and upward-continued gravity models. This was the second flight in a series, and was intended to (1) test the use of differential GPS tracking, and (2) measure gravity at altitude.</p> <p>A balloon operates in a largely unpredictable environment, where little, if any "ground truth" data are available. The motions of the balloon must be very accurately accounted for in gravity estimation; the experimental package contained a full complement of inertial sensors, radar transponder, a GPS receiver, and a gravimeter. The first flight in October 1983 showed that tracking was the most difficult problem; the second flight included differential GPS tracking to overcome that problem. The flight was successful with GPS tracking and gravity measurements. Keywords: Global positioning system;</p>					
20. DISTRIBUTION/AVAILABILITY OF ABSTRACT <input checked="" type="checkbox"/> UNCLASSIFIED/UNLIMITED <input checked="" type="checkbox"/> SAME AS RPT. <input type="checkbox"/> DTIC USERS			21. ABSTRACT SECURITY CLASSIFICATION Unclassified		
22a. NAME OF RESPONSIBLE INDIVIDUAL Andrew R. Lazarewicz			22b. TELEPHONE (Include Area Code) (617) 377-5255		22c. OFFICE SYMBOL AFGL/LWG

A

Preface

The Air Force Geophysics Laboratory initiated the balloon-borne, high-altitude, gravimetry experiment to satisfy a Department of Defense (DoD) requirement. DoD's Defense Mapping Agency develops the gravitational model used with strategic missile systems. It is important to verify the accuracy of this model at various altitudes, particularly near missile launch sites.

We thank Dr. Donald H. Eckhardt, Director, Earth Sciences Division, and Dr. Thomas P. Rooney, Chief, Geodesy and Gravity Branch, for their unrelenting patience and guidance with this project and report.

Accession For	
NTIS GRA&I	<input checked="checked" type="checkbox"/>
DTIC TAB	<input type="checkbox"/>
Unannounced	<input type="checkbox"/>
Justification	
By	
Distribution/	
Availability Codes	
Dist	Avail and/or Special
A-1	



Contents

1. INTRODUCTION	1
2. EXPERIMENTAL DESIGN	6
2.1 Gondola Design Concept	6
2.1.1 Gondola Configuration, Flight H85-20	10
2.2 Flight Control and Data Systems	10
2.3 Sensors	12
2.3.1 Vibrating String Accelerometer (VSA)	12
2.3.1.1 Mechanical Layout of the System	13
2.3.1.2 VSA System Description	13
2.3.1.3 Method for Frequency Counting	16
2.3.2 Motion-Sensing Instrument Package	16
2.3.2.1 Instruments	17
2.3.2.2 System Description	17
2.3.2.3 Calibration	18
3. FLIGHT OPERATIONS, FLIGHT H85-20	19
4. DATA ANALYSIS	19
4.1 Introduction	19
4.2 Tracking	22
4.2.1 Radar	22
4.2.2 GPS	23
4.3 Balloon Dynamics	24
4.4 Data Processing	30
4.5 Data Analysis	42
4.5.1 Quick Look	42
4.5.2 Detailed Look	45
REFERENCES	49
LIST OF ACRONYMS	50

Contents

APPENDIX A:	Relative Gravity Measurements at Holloman AFB, NM	51
APPENDIX B:	Science and Balloon-Control Data Stream	53
APPENDIX C:	Instrument Calibration Table	57

Illustrations

1.	A Sketch of the Balloon Gravity Concept	3
2.	A Sketch Showing Exaggerated Motions of the Instrument Package	4
3.	Typical Winds Over Holloman Air Force Base are Shown	5
4.	A Sketch Showing the Construction and Layout of the Gondola Package	8
5.	This Photograph Shows the Swivel Attachment to Minimize Gondola Rotations During Flight	9
6.	The Flight-ready Gondola on the Launch Pad	11
7.	A Sketch of the Vibrating String Accelerometer (VSA) Sensor	14
8.	A Sketch Showing the Communications and Tracking Systems Used During Flight	20
9a. & 9b.	Samples of X and Y Acceleration Data as Recorded in the Gondola	25
10a. & 10b.	Samples of X and Y Gyro Data as Recorded in the Gondola	26
11.	Cross-correlation of X and Y Gyro Data	28
12a. & 12b.	Cross-correlation of the VSA With the X and the Y Gyro Data	29
13a. & 13b.	VSA Gravity Data Compared With the Modeled Data Based on GPS Tracking Data	32 & 33
14.	The Difference of VSA Minus Model Gravity Data	34
15.	The Difference of BSA Minus Model Gravity Data With the VSA Being Delayed by 3 Seconds	35
16.	Differenced Data From Figure 15 With the First Level of Spike	36
17.	Differenced Data From Figure 15 With the Second Level of Spike	37
18.	Differenced Data From Figure 15 With the Second Level of Spike Removal and Smoothed in One Pass	38
19.	Differenced Data From Figure 15 With the Second Level of Spike Removal and Smoothed in Twenty Passes	39

Illustrations

20.	Mean of Difference Array vs Number of Smoothing Passes	40
21.	Variance of Difference Array vs Number of Smoothing Passes	41
22.	Quick Look at About 35 Minutes of Data: (a) GPS Geodetic Altitude; (b) Gravitation Model Based on GPS Positions; (c) Gravity Model Based on GPS Tracking of Position, Velocity and Acceleration; (d) Gravity as Measured by the VSA; (e) Gravity Model Minus VSA; and (f) Gravity Model Minus VSA With the Model Being Advanced by 3 Seconds	43 & 44
23.	Slopes and Means of Subarrays 1 to 16	48

Tables

1.	Data Points Used for Statistical Test 1	45
2.	Data Points Used for Statistical Test 2	46

Balloon-Borne, High-Altitude Gravimetry The Flight of DUCKY II (October 1985)

1. INTRODUCTION

Gravity field values at high altitudes, between altitudes for aerial surveys and satellite orbits, (for example, 30 km), are normally estimated from upward continuation of surface measurements, downward continuation of satellite measurements as computed from orbital perturbations, and/or geoid models. These techniques are well-developed with generally accepted results, but are subject to some limitations. Upward continuation depends upon the quality and distribution of surface data, usually nonuniformly spaced, and taken from different surveys; thus, gaps, and uneven spatial distribution may result inaccurately upward continued estimates. With increasing altitude, short wavelength information on crustal structure is attenuated, not recoverable from downward continuation from satellite altitudes. Geoid models tend to emphasize wavelengths longer than about 30 km, and are well-known only over oceanic areas.

Verifying gravity data bases and models requires establishing the validity of the models at locations where measurements have not been made. While such models currently can be tested effectively at ground level, their validation at altitude awaits the development of a suitable approach. The Air Force Geophysics Laboratory (AFGL) has developed a program to verify gravity model estimates by

(Received for publication 26 October 1987)

measuring gravity directly using high-altitude balloons. The basic concept is shown in Figure 1. A gravimeter package suspended beneath a balloon is in a dynamic and largely unpredictable environment, sensing not only the gravitational acceleration of the earth but also all accelerations due to the motions of the balloon system. An exaggerated sketch of kinematic balloon motion is shown in Figure 2. For a specified time interval (for example, 1 second) during which a measurement is made, the variation in balloon accelerations is expected to be significantly greater than the variation expected in the Earth's field. Therefore, additional instrumentation is required to measure as many balloon motions as possible, such as rotation, bobbing, and swaying. As all such ancillary sensors are dependent on the local inertial frame, gravitational acceleration cannot be separated from vertical balloon accelerations without additional data acquired independently of the balloon's reference frame.

These independent data are extracted from balloon tracking which must accomplish three objectives: (1) the measurement of the gravimeter package accelerations (especially the vertical) referred to a ground-based coordinate system; (2) the measurement of velocity for estimation of the Eotvos effect; and (3) the measurement of the gravimeter position, which is used as an input to the gravity model. Combining balloon data with tracking data allows the separation of balloon-induced accelerations from gravitational accelerations.

The long-term goal is to determine gravity to 1 mGal (10^{-3} cm/sec²), and in support, obtain instrument motion data (worst-case limits) of accelerations to 1 mGal, velocity to 5 cm/sec, and position to 3 m in all three orthogonal coordinates.

The balloon launch was set to coincide with the lowest seasonal wind velocities (Figure 3) over Holloman Air Force Base where AFGL has its permanent balloon-launch facility. The mild wind velocities are desired to provide the most benign environment possible during the testing phase so that the analysis effort may focus on the performance of the gravimeter system. Balloons have been flown up to 150,000 ft where the air pressure is less than 1 mm of Hg. Temperatures can range from -70° C at night to almost 40° C on exposed parts of the gondola's aluminum framework in the daytime. The instrument packages had to withstand the shock and vibration associated with both launch and landing. Even with a parachute and a crush pad on the gondola, accelerations up to 8 g may be expected on landing. Ideally, the instrument packages would be self-contained except for telemetry and batteries.

The instruments were also operated in a strapdown mode; that is, the instrument axes are not fixed with respect to inertial space but are attached to the instrument package itself. Since the packages are rigidly fastened to the balloon gondola, the instrument axes correspond to a local coordinate system in the gondola.

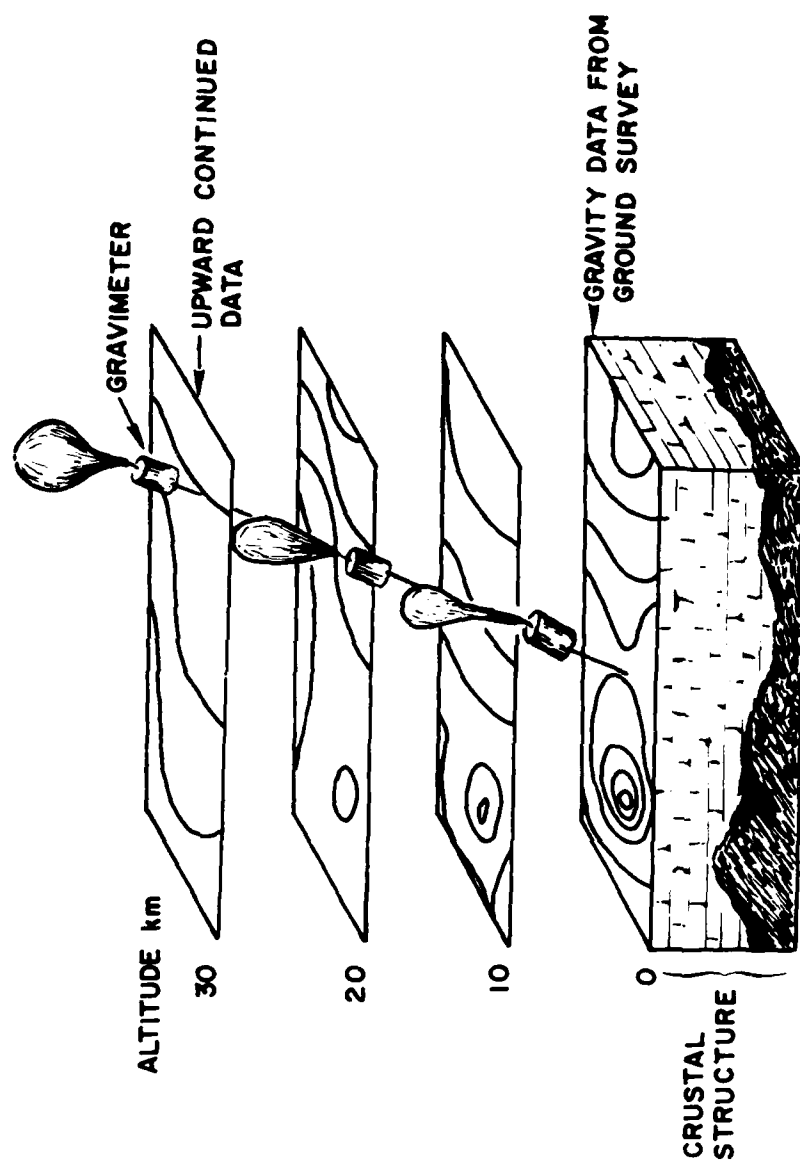
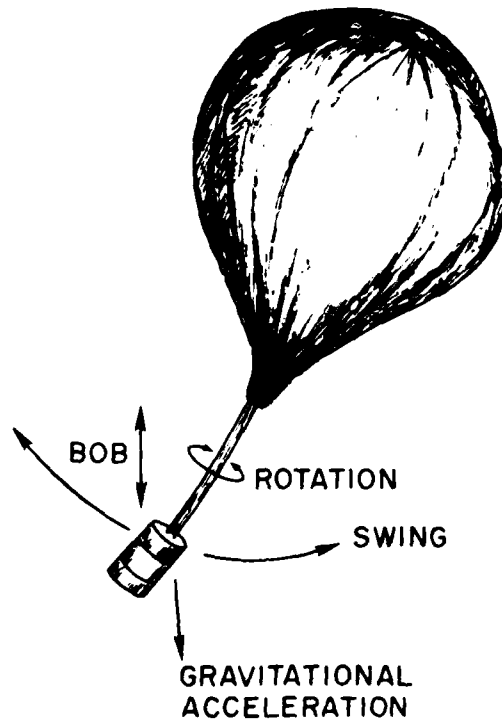


Figure 1. A Sketch of the Balloon Gravity Concept. Gravity data is upward continued from the surface, and tested at altitude from a balloon-borne platform

BALLOON GRAVITY



- GRAVIMETER MEASURES ACCELERATIONS DUE TO GRAVITY AND BALLOON MOTIONS
- INDEPENDENT MEASUREMENT OF BALLOON MOTION IS REQUIRED

Figure 2. A Sketch Showing Exaggerated Motions of the Instrument Package. Each of these motions contributes to a vertical acceleration term; thus, confusing the gravimeter data

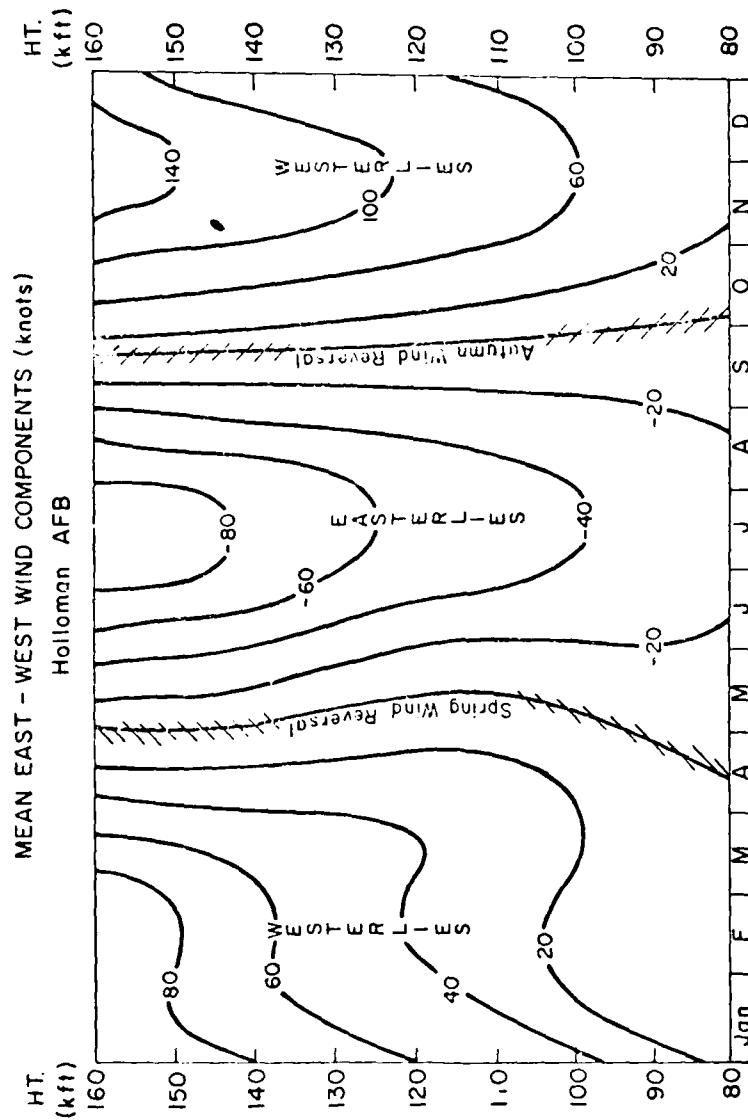


Figure 3. Typical Winds Over Holloman Air Force Base are Shown. To minimize balloon and gondola motion, flights are planned to occur during the seasonal wind reversals

2. EXPERIMENTAL DESIGN

2.1 Gondola Design Concept

The scientific goal was to resolve accelerations in the X, Y and Z axes to one part in 10^6 . Therefore, every effort was made to minimize (and measure) extraneous motion and to attempt to achieve a payload configuration that would hang beneath the balloon as close to vertical as possible. The gondola was a symmetrical shape, a cylinder, to reduce the effect of wind and turbulence.

Attachments were designed to limit the tendency of a lengthy flight train (the balloon-recovery parachute-gondola) to wind up and unwind as the system ascends to float altitude. During ascent, the balloon changes shape as it rises and imparts rotation to the system, storing this energy in the in-line, that is, extended, nylon recovery parachute. The mechanical aspects of the flight system design thus became paramount considerations to minimize undue linear motions and rotation. The design emphasized maintenance of balance and verticality during operation of any on-board control devices such as ballast dispensing and valving off helium lifting gas.

The melding of several independent, though closely interrelated subsystems necessitated devising a gondola system that could provide sectional disassembly and operational independence for service and individual testing and calibration, yet permit flexibility for modification. The size and form factor of the gondola were also limited by the launching method. A dynamic launch, with the gondola suspended from the boom of a mobile 30-ton crane, limits the vertical dimension that can be handled safely. Using a 2.9 million cu ft balloon the payload weight had to be kept under 2500 lb including 445 lb of pourable glass ballast, to reach the desired float altitude.

The stacked, cylindrical-section design concept for the aluminum gondola used in 1983 proved to be very satisfactory. For the 1985 flight some alterations were made as a result of our experience using it, and also to accommodate the addition of TI-4100 Global Positioning System instrumentation. The cylinder diameter was increased by 2 inches, the overall length decreased by 8.5 inches, and the number of cylindrical sections was reduced from 5 to 4. It was of great importance to retain the smooth cylindrical gondola exterior which could be covered by a tight, reflective insulating jacket. The flanges of the individual sections that were bolted together were redesigned, allowing the bolts to be accessible through ports from the outside. Instrument packages were easily positioned and removed by rack slides installed in the redesigned gondola sections. These changes greatly expedited the repeated gondola assembly-disassembly operations during testing

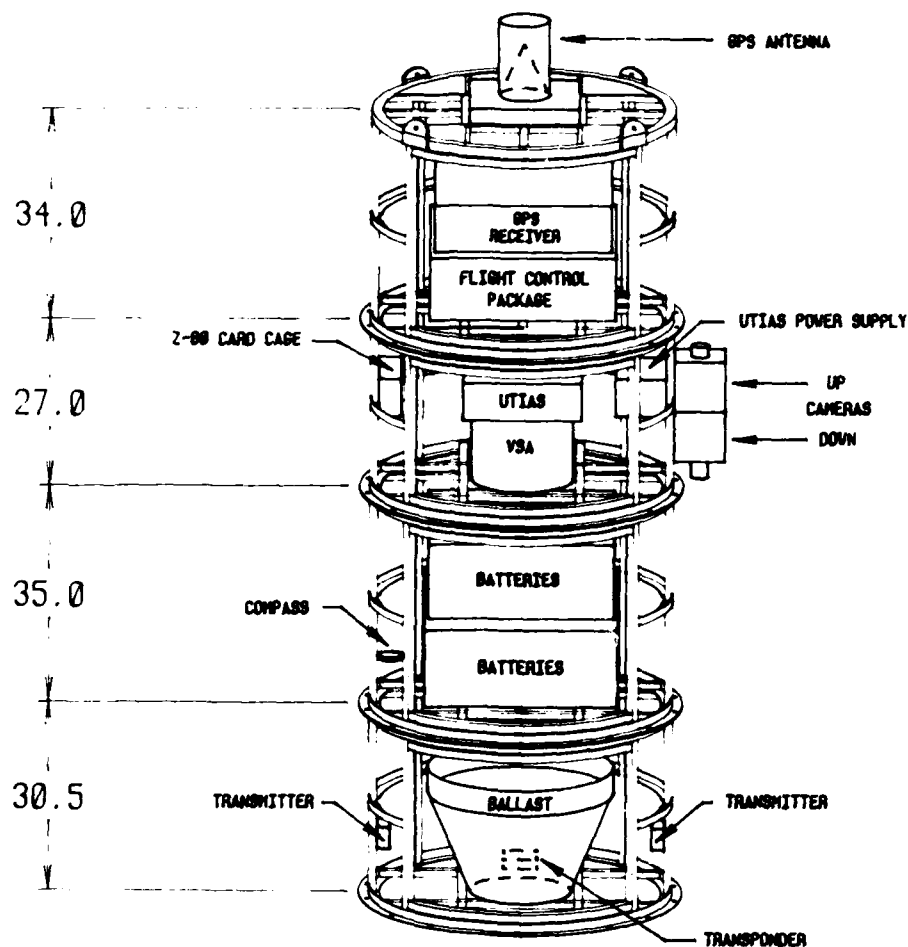
and calibration of the instruments in the various payload sections. The dimensions of the 1985 gondola are indicated on the sketch, Figure 4.

On both flights the gondola was attached to the load line through a four-point cable suspension. The suspension terminated in a singlepoint fixture for attachment to the launch crane's tri-plate release device. In 1985, a conical, omni-directional GPS antenna/preamplifier unit was mounted on the top face of the gondola. To prevent multipath reflections of the satellite signals to this antenna from the four-point suspension cables, the steel wire cables were replaced by Kevlar.

In order to decouple the payload from the sporadic rotations of the balloon/loadline system during float, for the 1985 flight a swivel assembly was inserted between the payload suspension and the parachute risers. The swivel assembly included slip-ring electrical connectors to the upper balloon-system controls. The prelaunch photo, Figure 5, shows the black swivel case between the tri-plate (held in the jaws of the launch crane) and the triangular attachment for the two bundles of parachute risers.

The parachute was specifically oversized to slow the impact velocity to 15 to 20 ft/sec, and a crush pad of stepped, corrugated cardboard 16-in. thick was attached at the base of the cylindrical gondola. A roll bar (impact-absorbing crush ring) 7-ft in diameter, concentric with the cylinder axis, assured that with anticipated horizontal velocities of 30 to 50 ft/sec, the gondola would lie over safely with minimal physical damage upon ground impact. The base of the crush pad carried impact switches designed to release one set of parachute suspension-harness risers to collapse the chute and prevent the possibility of dragging the payload across the ground after impact.

The exterior of the cylindrical gondola was skinned with aluminum. When flight-ready, it was wrapped with 2-in. thick fiberglass "Certainteed" pipe insulation, with an All Service Jacket (ASJ) vapor barrier of aluminum foil. A glass-reinforced, whitecoated Kraft laminate, was installed to serve as a reflective, white outer surface, finished with superior compression resistance for added protection.



GRAVITY MEASUREMENTS GONDOLA

FLIGHT H85-20

Figure 4. A Sketch Showing the Construction and Layout of the Gondola Package. It is designed to keep the vertical axis of the gondola as close to vertical as possible.



Figure 5. This Photograph Shows the Swivel Attachment to Minimize Gondola Rotations During Flight. The parachute harness is connected on the left; the gondola is hanging below on four Kevlar shrouds; the tip of the launching crane is on the right. All three are connected to a corner of the tri-plate

2.1.1 GONDOLA CONFIGURATION, FLIGHT H85-20

The top section of the assembled gondola, Figures 4 and 6, contained a 5-channel TI-4100 Global Positioning System receiver/processor, its Rubidium clock, the AFGL flight control package and a power patch panel. The TI-4100 GPS receiver/processor was mounted on a thick aluminum plate to dissipate its considerable heat output. The Rubidium clock was separately shock-mounted in the same section.

In the section immediately below were the Vibrating String Accelerometer (VSA), its card cage, the UTIAS motion sensors package and separate power supplies for the VSA and UTIAS sensors. Two Canon F-1 cameras were carried in an insulated box attached to this section.

The battery power for the complete balloon system was packaged in two "freeze pack" containers, one atop the other, on rack slides in the third section. The magnetic compass was also housed in this section.

The bottom section had the valve-controlled hopper carrying pourable glass bead ballast, the primary and secondary telemetry transmitters, and the FAA transponder for emergency tracking. Attached to the base of this section were the crush pad, and, around its perimeter, the four impact switches. The antennas for the primary command-receiver and two telemetry transmitters were mounted on PVC pipe beneath the crush pad. The back-up command-receive antenna was a blade type, mounted to the crushable aluminum outer roll ring to preserve command-control in case the bottom antenna was damaged at launch.

2.2 Flight Control and Data Systems

The design of the flight-control system followed the standard AFGL practice of providing primary and backup systems to ensure positive experiment control and redundant flight-safety control via separate power systems. A single instrument frame housed all flight-control electronics, two digital command units, housekeeping sensors and monitors, power control interface units and two data encoders. This instrument frame was enclosed in a laboratory-grade, low-temperature-insulated container (bio specimen "freeze pack") for environmental protection and temperature control. This method of packaging has very high flexibility. The final configuration is an assembly of modular items, all interconnected by a master harness terminated in a master patch-panel-type connector interface for inputs and outputs.

The twenty-eight 80Ah BB622/U batteries were configured to provide six isolated power sources for the various instruments and sensors aboard.

A continuous digital command up-link on 423.5 MHz was used for flight and experiment control.



Figure 6. The Flight-ready Gondola on the Launch Pad. The small cylinder on top houses the GPS antenna; white insulation encases the gondola; the crushable landing ring is around the second section from the top; the landing crush pad, contact switches and antennas are on the bottom. The parachute shrouds and control cable to the balloon systems are on the right; the tip of the launching crane is at the upper left.

The addition of the on-board TI-4100 GPS receiver/processor for Flight H85-20 led to significant changes in the data-recovery systems. One of the two telemetry downlinks was dedicated to the GPS system. All of the VSA measurements, motions-sensing, housekeeping and monitoring data were transmitted on the other (the "science" downlink). Both data streams were serial, asynchronous transmissions on the 2.2 GHz band, Frequency Shift Keying (FSK) encoded, and RS-232 driven; the GPS data at 4800 baud, the "science" measurements at 9600 baud. The "science" data were encoded in an 8-bit word, 88-word frame format. These word assignments are listed in Appendix B. To time-correlate the science data stream with the GPS tracking measurements, readout of the science data frame was strobed by a 1 Hz, 10 msec pulse output from the GPS receiver. This pulse indicates the moment (within 20 msec) when the GPS receiver has made a navigation measurement. This signal was used to synthesize a 10 Hz pulse which was monitored by a Z-80 microcomputer to initiate readout of all the analog-to-digital "science" measurements, followed by the balloon-system digital monitors. The Z-80 also transfers the ASCII-encoded GPS time of the 1 Hz pulse (GPS seconds of the week) from the GPS receiver to the "science" downlink so that all of the data are properly time-tagged.

The VSA measurement was transmitted in eight, binary-coded-decimal (BCD) digits, with two BCD characters to an 8-bit telemetry word. Each of the analog-sensor measurements—from the gyros, accelerometers, voltages, temperature, and so on—was binary-coded in two, 8-bit telemetry words. Each individual bit of Words 85-88 was a digital, status indicator, described in the Word Assignment listing, Appendix B.

At the ground station, the two telemetry downlinks were separately received, recorded on analog magnetic tape, FSK demodulated and fed via RS-232 lines to the PDP-11 computer and to several Zenith-100 PC's for selective real-time, quick-look data displays. The PDP-11 output selected data output from the "science" telemetry to CRT displays and printers and recorded the data format on digital tapes.

2.3 Sensors

2.3.1 VIBRATING STRING ACCELEROMETER (VSA)

The Vibrating String Accelerometer (VSA) is a single-axis accelerometer originally designed for the Atlas missile navigation system in the 1960s. When the VSA was deemed obsolete for the Atlas, the Woods Hole Oceanographic Institution (WHOI), Woods Hole, MA acquired a collection of VSAs from

government surplus stock. WHOI developed and built a shipborne gravimeter system based on the VSA,^{1, 2, 3} and successfully used it in geophysical research over the subsequent years. When the balloon-gravity programme came into being, WHOI proposed to build a gravimeter/inertial system for AFGL. In March 1983, WHOI came under contract to AFGL and successfully built a gravimeter system in time for the October flight of DUCKY IA.⁴

2.3.1.1 Mechanical Layout of the System

Six basic modules were developed at WHOI and placed aboard the gondola:

(1) The VSA and Oven System: a "can" (VSA two-stage oven) housing the VSA and its temperature-control components and circuitry; (2) The Processing System: a cardcage holding six circuit cards; (3) The Oscillator: a shielded "cube" holding two more cards: a 10 MHz crystal oscillator and associated oscillator control circuitry; (4) The Encoder: (obtained from AFGL) that relayed acquired VSA data to ground; (5) The Heat Sink: a large heat sink upon which were mounted both a power supply that converted power from the AFGL batteries for use in VSA circuitry, and a set of power transistors used to drive VSA heater blankets; and (6) The Front Panel: used for monitoring and adjusting VSA components while the system was on the ground.

2.3.1.2 VSA System Description

The principal component of the can are: (1) VSA Sensor: The VSA is a device consisting of a mass suspended by two metal bands (strings) under tension (Figure 7). The tension on, and the length of, each string is set so the resonant frequency is about 4 kHz at a very high Q (value not available). Due to the high Q, the strings will oscillate (at resonance) very easily, and ambient noise is enough to drive the oscillations. The surrounding magnets sustain the oscillations.

1. Bowin, C.O., Wing, C.G., and Aldrich, T.C. (1969) Test of the MIT vibrating string gravimeter, J. Geophys. Res. 74, 12:3278-3280.
2. Bowin, C.O., Folinsbee, A., and Aldrich, T.C. (1970) Test of digital VSA sea gravity meter and comparison with LaCoste and Romberg gyro stabilized gravity meter (Abstract), Trans. Am. Geophys. Union 51, 4:261.
3. Bowin, C.O., Aldrich, T.C., and Folinsbee, R.A. (1972) VSA gravity meter system: tests and recent developments, J. Geophys. Res. 77:2018-2033.
4. Lazarewicz, A.R., Schilinski, B.J., Cowie, R.J., Rice, C.L., Moss, P., and Carter, L.N. (1985) Balloon-Borne, High-Altitude Gravimetry, The Flight of DUCKY IA (October 1983), AFGL-TR-85-0342, ADA 169942.

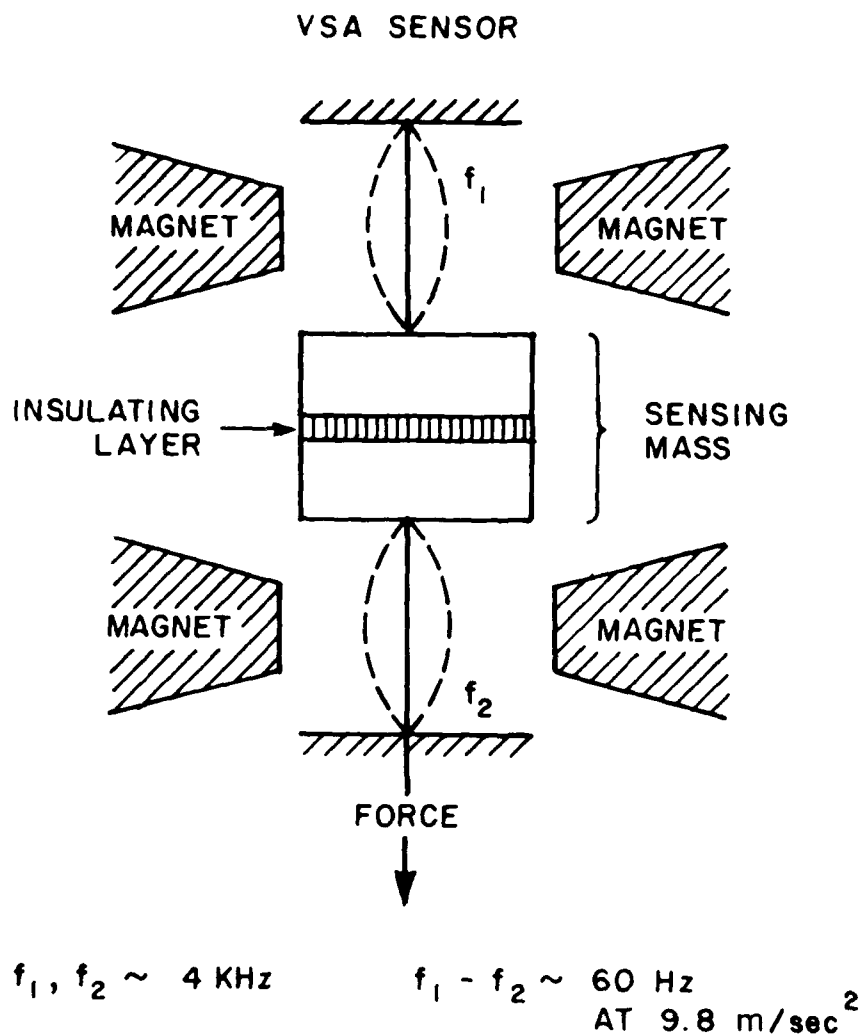


Figure 7. A Sketch of the Vibrating String Accelerometer (VSA) Sensor. Two metal strings under tension are separated by a mass. A force acting on the mass along with the strings will cause different tensions on each string; thus, each string will have a different resonant frequency. The VSA system measures the acceleration from the beat frequency of the two strings. The resonant frequency of each string is about 4 kHz; the beat frequency at 1 g is about 60 Hz

The oscillation creates an electromagnetic force (EMF) due to the ambient magnetic field. The EMF is sensed, amplified, and fed back to the strings. When an acceleration is sensed in the sensitive axis (along the strings), the force acting on the mass results in different tensions acting on the two strings. The string in the direction of the acceleration is at a lower tension than the opposite string. At 1 g, the difference in resonant frequencies is about 60 to 64 Hz. Thus, when the two frequencies are mixed, three narrow bands of frequencies exist: 65 Hz, 4 kHz, and 8 kHz. When low-pass filtered, the final VSA output frequency is about 65 Hz, and it is this frequency that is a measure of the along-axis acceleration. For this flight, we chose to sample the VSA output every 10 cycles, giving an effective sampling rate of about 6.5 Hz. The circuitry was designed to yield either a frequency count or the period, the latter being the choice for the flight.

(2) Osc/Amp: An Oscillator/Amplifier circuit effectively sustains oscillations in one of the two strings of the sensor by positive feedback. The output of the circuit is a sinusoidal signal with a nominal frequency of 4.5 kHz. There are two of these circuits in the can, and two strings in the sensor. The difference in the frequency of the two resulting signals is directly proportional to the acceleration and/or the component of gravity experienced along the input axis of the sensor: $a = K f_d + B$, where a is acceleration in milligals, K is the scale factor, f_d is the difference frequency in Hz, and B is a bias term in milligals. Prior to the experiment, a scale factor determination was performed, and the following values obtained:

$$K = 15240.94 \text{ (milligals/Hz)} \quad (1)$$

$$B = 4330.71 \text{ (milligals)} . \quad (2)$$

A rough value for f_d at 1 G acceleration is 64.1 Hz. (3) Inner and Outer Ovens: A two-stage oven is used to maintain the temperature of the sensor; the "outer" housing the "inner." Each oven contains two thermistors that sense temperature within the controlled volume: a "monitor" thermistor that is used solely for temperature observation, and a "control" thermistor that is connected in a bridge configuration with high-quality resistors and connected to a preamp mounted in the can. This circuitry is used for controlling the temperature by regulating the power supplied to heating blankets mounted around each oven.

2.3.1.3 Method for Frequency Counting

Since the value of f_d at 1 g is roughly 64.1 Hz, the PLL chip outputs a square wave of 256 kHz mean frequency. By its very nature, the frequency counting technique averages the desired information over the gate time, but also performs some analog filtering of the data. This technique provides a convenient, fairly high resolution representation of the average frequency of f_d , with the disadvantages of observation of f_d through a "fuzzy" window caused by the nonlinearities in the analog filtering of the PLL, and the phase-detector stages of the chip. In order to provide a less processed data set for the balloon experiment, the period counting method was actually used.

At certain times, however, it was advantageous to use the frequency counting data for on-the-ground testing, since a direct display of the accelerations experienced by the sensor ($4096 f_d$) was available in real time.

In period counting, as in frequency counting, frequency variations of f_d are averaged over the time between N zero crossings. N was 10 during the actual flight, so that averaging time at 1 g acceleration was 10. (1/64.1) or roughly 156 msec. Less filtering would have been accomplished for N=1, but then the data rate would have been too high for the acquisition system. With this method, no other filtering was done, so a "purer" form of acceleration data was recorded. One drawback of this approach is the fact that data were sampled at irregular intervals. An interpolation scheme using bilinear interpolation was used to produce a constantly sampled data stream amenable to further processing techniques.

2.3.2 MOTION-SENSING INSTRUMENT PACKAGE

The UTIAS flight-test package⁵ consisted of three rate gyros and three accelerometers. The rate gyros were mounted with their axes orthogonal to each other, and would measure the pendulation and rotation rates with respect to a set of axes fixed to the instrument package. Relative angular displacements would be obtained by integrating the gyro rates. The vertically mounted accelerometer would sense the balloon's vertical acceleration superimposed on the earth's gravitational field. After removing the gravity signal from the measurements, they could be integrated twice to yield relative vertical displacements. A three-axis magnetometer that detects the components of the earth's magnetic field about three orthogonal axes was also included in the balloon motion-sensing package.

5. DeLeeuw, J. H., and Kung, W. L. (1984) Development of motion-sensing package for high-altitude balloons, University of Toronto Institute for Aerospace Studies, AFGL-TR-85-0258, ADA 170225.

2.3.2.1 Instruments

Rate Gyros: The three rate gyros in the original motions-sensor package developed by the University of Toronto Institute of Aerospace Studies (UTIAS) were replaced for the 1985 flight by more sensitive GNAT miniature rate gyros. A torsion bar spring is used to provide a restoring torque about the gyro's precessional axis so that the precession rate is proportional to the input rate. The rate of precession is detected and converted to an electrical signal by the signal generator/pickoff. Two rate gyros, designated X and Y, were assigned to detect balloon pendulation. The other rate gyro, called the Z-gyro, was used to measure the rotation of the payload about its vertical axis.

Accelerometers: The vertically mounted or Z-accelerometer should be able to sense the up-and-down motion of the balloon system. Assuming sinusoidal motion, the maximum accelerations involved are a few hundredths of one g. The accelerometers are Sundstrand QA1100s. The instruments are force-feedback acceleration transducers that feature a completely elastic seismic suspension, made from amorphous quartz, that virtually eliminates bearing friction. The servo electronics are completely contained within the instrument, which also has a convenient self-test capability. The output voltage signal is developed across an internal load resistor.

Magnetometer: The three-axis magnetometer is a Schonstedt SAM-73C. It is a sensitive instrument and exhibits highly linear response on all axes. Its main purpose is to provide an absolute azimuth reference from measurements of the horizontal components of the earth's magnetic field.

2.3.2.2 System Description

The motion-sensing package hardware is housed in a pressure-tight aluminum enclosure. Adjustable pads on each corner and the two bubble levels enable the package to be leveled after mounting. The enclosure consists of a baseplate and a cover, with an O-ring providing the seal between them. There is a port on the cover that allows the package to be vacuum-tested. A pressure-tight container was necessary because the accelerometers were not hermetically sealed. This meant that changes in air pressure could affect the instrument's internal damping and, hence, its performance.

The accelerometers are housed in a triaxial mounting block of anodized aluminum fastened to a Lexan base. This base can be leveled independently of the aluminum baseplate. The arrangement for the rate gyros is similar. These sensors are surrounded on five sides by blue styrofoam walls that, with the Lexan plates, form an insulated compartment. The enclosure is heated to a constant

temperature of 50° C to prevent external temperature fluctuations from affecting performance. The "oven" is heated by a Darlington power transistor regulated by an on/off control circuitry. Two sensors provide a readout of the "oven" temperature, and the temperature of the rest of the instrument package.

The problem of maintaining this "oven" at a constant temperature over several hours is complicated by the fact that the rate gyros themselves are generating heat. Eventually, if this excess heat is not removed, the temperature cannot be regulated, and the sensors might be destroyed. For Flight H85-20, the inconvenient, frozen-chemical heat sink used on the first flight was eliminated. Instead, the power supply was removed from inside the oven, several copper straps were placed at opposite corners to conduct heat away from the baseplate, and the package covers were painted with flat black enamel.

2.3.2.3 Calibration

Magnetometers: No calibrations were performed for the three-axis magnetometer because of the lack of large Helmholtz coils. Instead, the manufacturer's calibration data were used to reduce the flight data.

Rate Gyros: The rate gyro calibrations were made using a Genisco Model C-181 rate table that is capable of rotating at rates from 0 to 1200 deg/sec in both clockwise and counterclockwise directions. The gyro to be calibrated had its sensitive axis aligned with the rotational axis of the rate table. This meant that a special mounting jig had to be used for testing X- and Y-rate gyros. Power and signal lines were routed through slip rings on the rate table. The high- and low-sensitivity rate gyro outputs were measured using a Hewlett-Packard true rms meter. Readings were obtained as the rate was increased in steps from 0 to 1 deg/sec and then decreased for both clockwise and counterclockwise rotation.

Accelerometers: Static calibration of the accelerometers was performed by tilting the package along the sensitive axis of each sensor, and measuring the component of earth's gravity. The experimental setup was similar to that used previously at UTIAS for calibrating the flight-test package. The instrument package was fastened to its mounting jig, and the whole assembly was clamped to a large turntable that could be rotated about a horizontal axis. The sensor outputs were read out on a true rms meter.

3. FLIGHT OPERATIONS, FLIGHT H85-20

Flight preparations at AFGL Detachment 1, Holloman AFB, NM occurred in two stages. During 22 September - 11 October 1985, the various sensors were recalibrated and instruments interfaced with telemetry and command systems. With a prolonged period of bad weather forecast and scheduling conflicts on the range, the launch was postponed and personnel departed for home stations. During 23-25 October 1985, the final systems checkouts, launch and flight were accomplished.

The 2.9 million cu ft balloon was launched from Nenninger Launch Site on Holloman AFB, NM at 14:24 Zulu time (0824 MDT). The scheduled launch had been delayed one hour due to high surface winds and a temperature inversion that would appreciably reduce lift on the balloon: winds at the 300-400 ft level were 15 kt and there was a 22° F temperature inversion above 300 ft. After sunrise, however, the winds subsided to an acceptable 10-11 kt. Helium inflation was increased to provide 12 percent free lift. The launch was smooth and the system penetrated the inversion at a good rate.

The balloon reached the 98 Kft float level at 15:58 Z. After two hours the helium valve was commanded open for several 5-6 min periods followed by 1-min intervals of "ballast pour" to cause the balloon to descend and level off at the 80 Kft level. Flight was terminated at 20:47 Z. The payload landed 17 miles ESE of the Roswell VOR station. The outer aluminum crush ring on the gondola collapsed upon impact, as designed, and all of the instruments were recovered in excellent condition.

4. DATA ANALYSIS

4.1 Introduction

The primary objective of this flight was to test the differential GPS tracking system; the secondary objective was to improve on the gravity field measurement shown to be feasible with the flight of DUCKY IA. As with DUCKY IA, a great deal of data were collected, organized, inspected and analyzed by several different groups. Overall, the flight, data collection and analysis went very well, but a few problems did complicate the data analysis sufficiently that the full promise of this experiment was not fulfilled. Nevertheless, we did succeed in demonstrating GPS tracking and improving the quality of the gravity measurement from DUCKY IA (Figure 8).

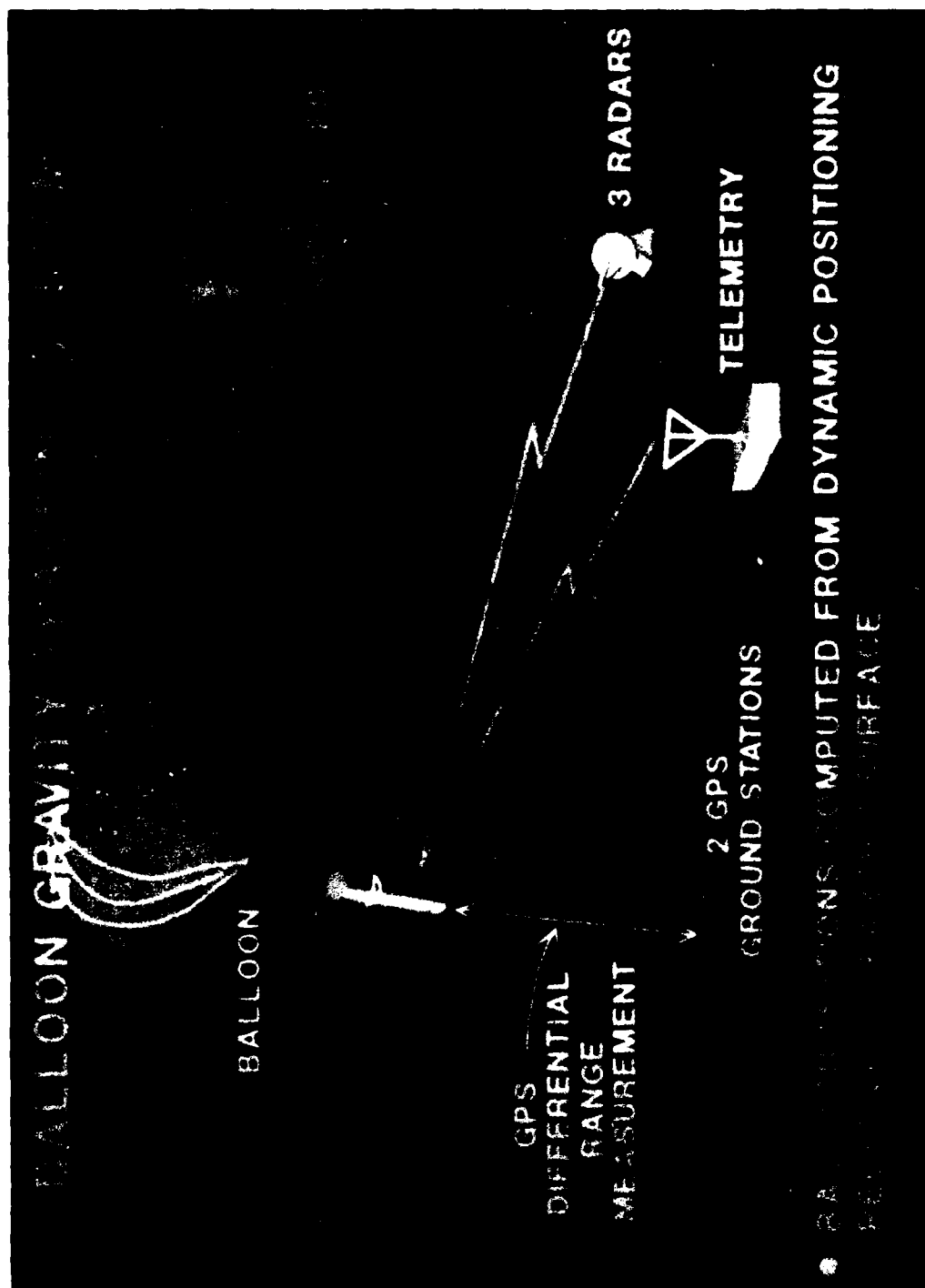


Figure 8. A Sketch Showing the Communications and Tracking Systems Used During Flight. A total of 4 GPS satellites, 3 ground radars (using both range and doppler tracking), 2 ground GPS stations, 2 telemetry stations on the ground, and the gondola system had to be all working simultaneously for successful recording of gravity data

The technical problems which affected the data analysis as we originally planned were: (1) data dropouts appeared in the ground station handling of the downlink data, (2) the radar tracking was shut off for a significant portion of the flight, (3) one of the GPS satellites used for tracking received the wrong ephemeris data uplinked from the GPS control ground station, (4) one magnetometer channel (Y-axis, a horizontal axis) did not work, and (5) a faulty ground wire inside the VSA sensor was not detected until after the flight causing some noise in that data. The goals we set, consistent with our resources were: complete coalescing the data into useable investigator data tapes, determine GPS tracking for the quietest period of time lasting more than 15 min, correct for translational motions of the experiment package (not rotational motions), and make our best estimate for the gravity values. Data collection during flight went smoothly, but telemetry dropouts proved to be a serious problem for real-time flight analysis which later affected both science and GPS post-flight data analysis. This flight was the first to use a digital telemetry link equivalent to a long RS-232 line, but we had the standard FM PCM data recordings for backup. The radar tracking gaps were not a significant problem as we used these data for validation of the GPS tracking data. The GPS ephemeris was recovered properly after the flight. The magnetometer channel was lost and thus made the magnetometer not useful in orienting the gondola with respect to the Earth's magnetic field. Since a magnetic compass did fly, the gondola could be oriented, about the vertical axis, with respect to Magnetic North. In fact, the Y-channel could be partially reconstructed from the two working channels and the compass. The VSA problem is not recoverable; this was unfortunate as the strength of the VSA lay in its ability to integrate over long periods of time without increasing the inherent instrument noise. The bad ground wire introduced spikes of a variety of amplitudes, making the timing of the VSA oscillators much more noisy. Although this problem should not affect the mean estimate of the gravity measurement, it does increase the uncertainty about the estimate.

It is not our intention to focus on these specific problems, but the reader should keep these problems in mind. It is important to understand that the capabilities of this instrument as it exists now are much greater than what we are able to report here.

4.2 Tracking

The principal limitation in high-altitude gravimetry, as concluded from the flight of DUCKY IA, is high accuracy tracking. Since all accelerometers measure only acceleration and cannot distinguish between gravitational acceleration and kinematic acceleration, it is critical to add sensors to aid in separating the two. There are only two known ways in which this can be done: (1) External tracking to directly determine kinematic acceleration; or (2) Gravity gradiometry to directly detect gravitational acceleration. External tracking works by measuring position, velocity and acceleration relative to the tracking device, which is fixed, usually in a non-inertial frame. Gravity gradiometry works by measuring gravity gradients. The flux of the gravity field is constant through any size shell surrounding gravitating body. As a result, the strength of the gravity field must vary with radial distance, since the area of a spherical shell surrounding a gravitating mass varies with radial distance. Therefore, all gravitating masses must have a radial gravity gradient. A mass undergoing kinematic, rectilinear acceleration, on the other hand, accelerates uniformly, and sees no gravity gradient. A sensor on a rotating mass senses centrifugal acceleration, which is a function of radial distance. Therefore a gravity gradiometer can sense rotation. Therefore, a gravity gradiometer will directly sense gravitational and rotational acceleration, but not translational acceleration. Adding a gyroscope measuring only rotation can resolve the ambiguity measured by the gravity gradiometer. So, in principle, there are the two ways to separate gravitational from kinematic acceleration. We chose external tracking via GPS because it is much simpler, and it has the potential to resolve 1 mGal accelerations with available technology. DUCKY II did have inertial sensors, and when properly combined with GPS, highly accurate tracking data is possible.

4.2.1 RADAR

The tracking system for DUCKY IA was accomplished using a multi-station solution from three White Sands Missile Range (WSMR) radars. These radars provided three-dimensional positions to an accuracy of about 4 meters in each axis. Velocity and accelerations were determined from the first and second derivatives of the position data. The data were recorded by WSMR and converted to a single multiple-station solution in WSMR coordinates (relative to a flat plane, tangent to the WGS72 ellipsoid at a point in WSMR). These solutions were converted to the geocentric and geodetic system by AFGL. This same system was used for DUCKY II with a few enhancements: (1) the radars in use were upgraded since DUCKY IA, and (2) Doppler radars were used to compute the line-of-sight velocity between the radar and experiment package. The Doppler data were not

used due to lack of resources, but are available for future use. A few hours of data are not available due to the unavailability of the radars, but the major purpose of verifying the GPS tracking system was well served.

4.2.2 GPS

GPS tracking for DUCKY II was accomplished using three DMA versions of the TI 4100 receivers, one in flight and two on the ground. The two ground stations were picked to minimize distance between ground receiver and balloon. For the flight, one ground station was placed at AFGL Det 1, near the launch site; and the other was placed on the roof of the Post Office in Lovington, NM, near the expected landing area. The data from the flight receiver was telemetered and analyzed in real-time, just as the ground stations; only the hard line was replaced with a radio link.

The Applied Research Laboratory (ARL), University of Texas at Austin, provided the GPS tracking support with the DMA Ti 4100 receivers in their care, in all aspects of the flight and analysis. Although some GPS satellites were tracked throughout most of the flight, only a one-hour period, beginning about 1717 UTC had the required four satellites and good geometry. During this same period, the balloon motion was at a minimum, and the radar tracking system was on. Data analysis focused on this one-hour period, and ARL provided all relevant GPS data processing for this period. Their results were provided to AFGL as position, velocity and acceleration; these data are used in the following sections.

At the time of flight, GPS was a pilot program, with only six satellites in orbit. GPS will not be a mature service until at least the late 1980's or early 1990's. When GPS is fully operational, this experiment could be repeated, with good satellite coverage and geometry, from launch to landing. As GPS time was limited, we intended to put the best coverage at altitude; future flights will cover the ascent—a time of high interest. The ascent time covers 25 to 30 km of vertical distance, and gravitational acceleration and gradient data would be most interesting. Currently, we have demonstrated that this system works.

4.3 Balloon Dynamics

The following comments and attached plots were generated from an examination of the telemetry data over the period 16:30 to 16:47 Zulu, which is prior to the 34-minute period of the Difference array (17:18 to 17:52) discussed in subsequent sections.

X and Y Accelerometers vs Time (Figure 9a and 9b):

The high frequency oscillations on both plots are about 14-15 seconds per cycle, which correspond well with the period T expected for balloon pendulous motions, where $T = 2\pi \sqrt{L/g}$, the effective length L being about 140 ft (4270 cm) and $g = 970 \text{ cm/sec}^2$ at altitude, giving $T = 13.2$ seconds. The lower frequency oscillations have a characteristic period of several hundred seconds, corresponding roughly with the vertical oscillations of 4 to 5 minutes due to balloon-atmosphere dynamics.

X and Y Gyros vs Time (Figure 10a and 10b)

The 14-second oscillations of Figure 1 are present here as well, but much more regular and pronounced. These two plots indicate that the gondola is swinging in an elliptical fashion, of varying ellipticity, since the root-sum-squared of the amplitudes of the two gyros together fluctuates much less over time than the X or Y gyro separate; therefore, the pendulous motion is essentially continuous and the distribution of motion in the X and Y axes varies over time scales of 100 to 200 seconds, going from roughly circular to linear motion and back.

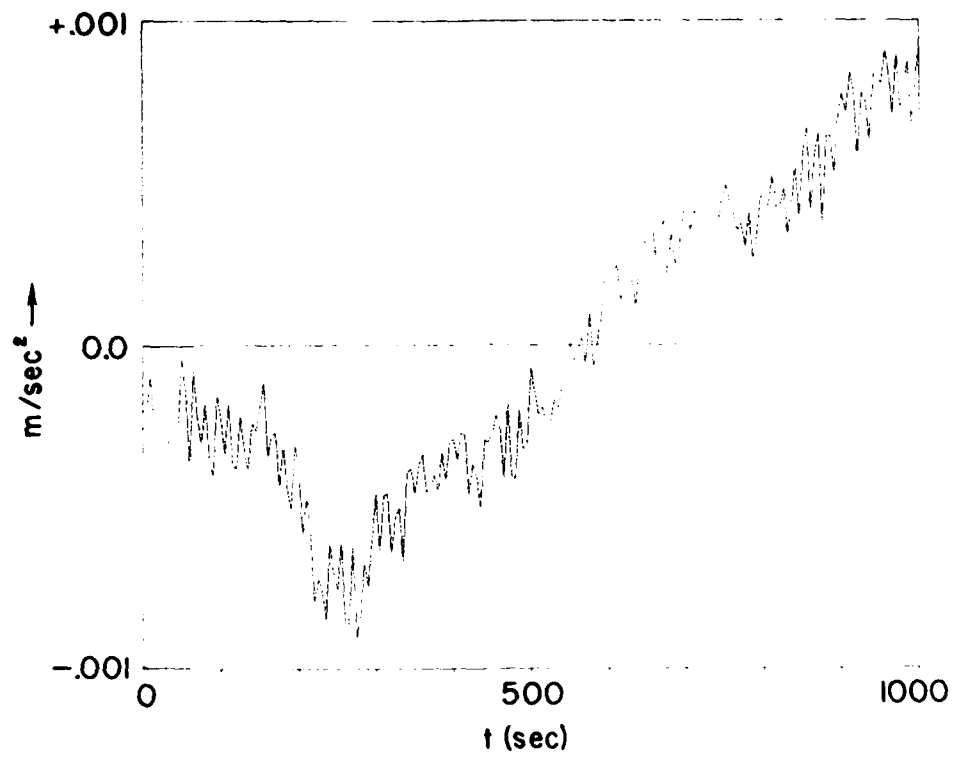
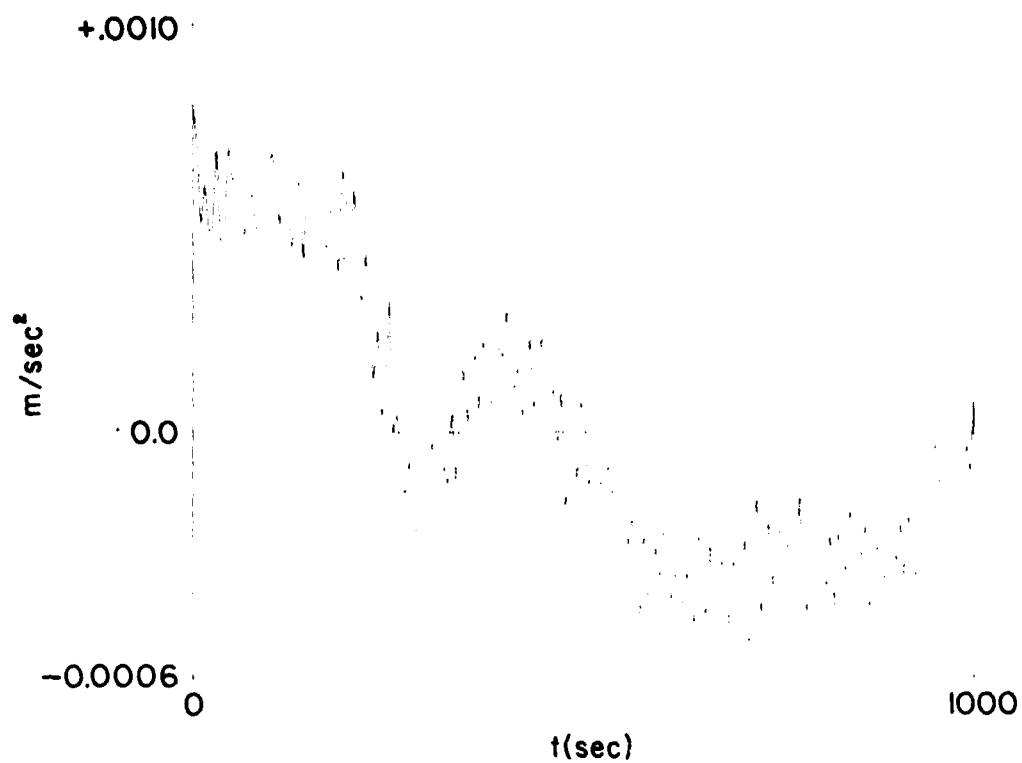


Figure 9a and 9b. Samples of X and Y Acceleration Data as Recorded in the Gondola

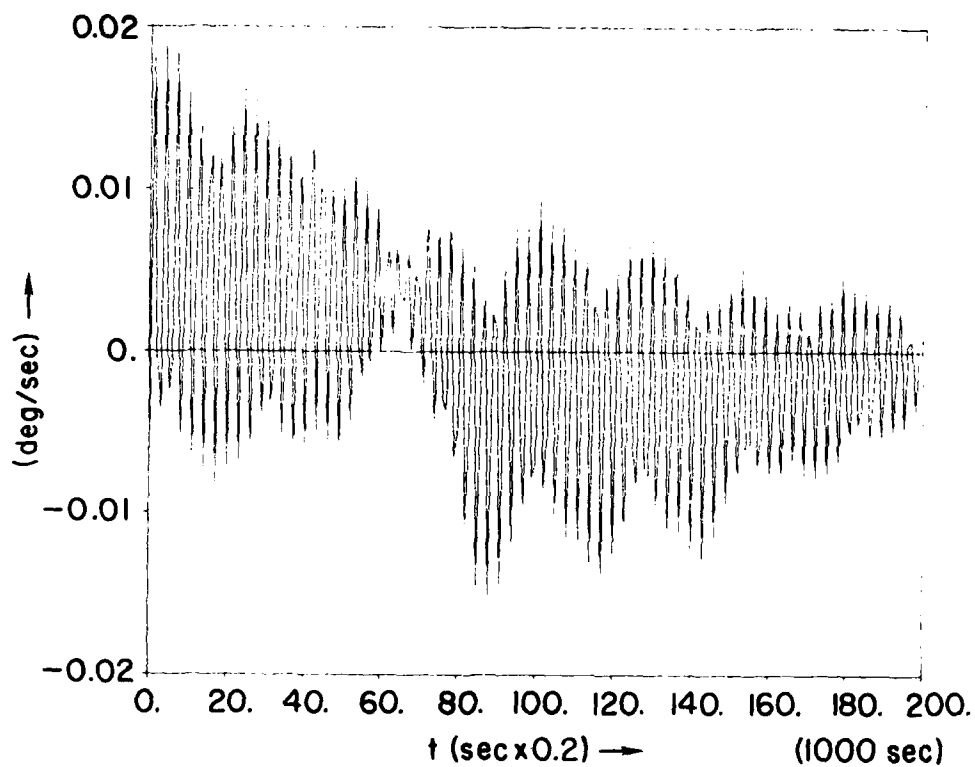
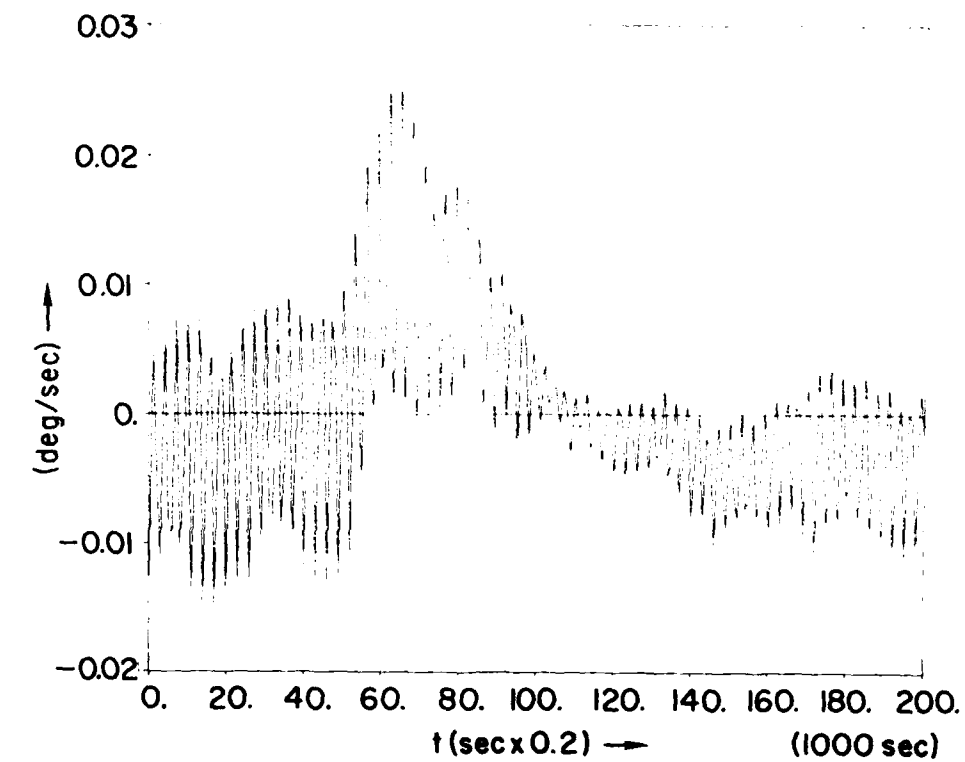


Figure 10a & 10b. Samples of X and Y Gyro Data as Recorded in the Gondola

X and Y Gyros Crosscorrelated (Figure 11):

This plot more than any other supports the notion of roughly circular pendulous motions having peak amplitudes of about 0.01 degree and a very regular period of 14.1 seconds (21-1/4 cycles in 300 seconds). Inspection of this plot allows one to gauge the ellipticity of the pendulous "orbits" of the gondola, since this would be inversely proportional to the peak amplitude for a given cycle. Obviously, the ellipticity varies by at least a factor of 2 over the 1000 seconds observed. The time scale of this variation of peak amplitudes, about 100 seconds, is indicative of how rapidly the plane of the major axis of pendulous motion rotates from one axis to another.

VSA Crosscorrelated With X Gyro and With Y Gyro (Figure 12a and 12b):

These two plots show the correlation between the vertical axis accelerations as sensed by the VSA, and the pendulous motions sensed by the gyros. The phase shifts between the two plots is about 70 seconds, with both plots showing a 70-80 second time interval to go from maximum to zero correlation. This time interval and phase shift, roughly equal, can be interpreted as the characteristic time for pendulous swings to rotate from one plane to another (90° rotation of the major axis), similar to the 100 seconds indicated from Figure 11.

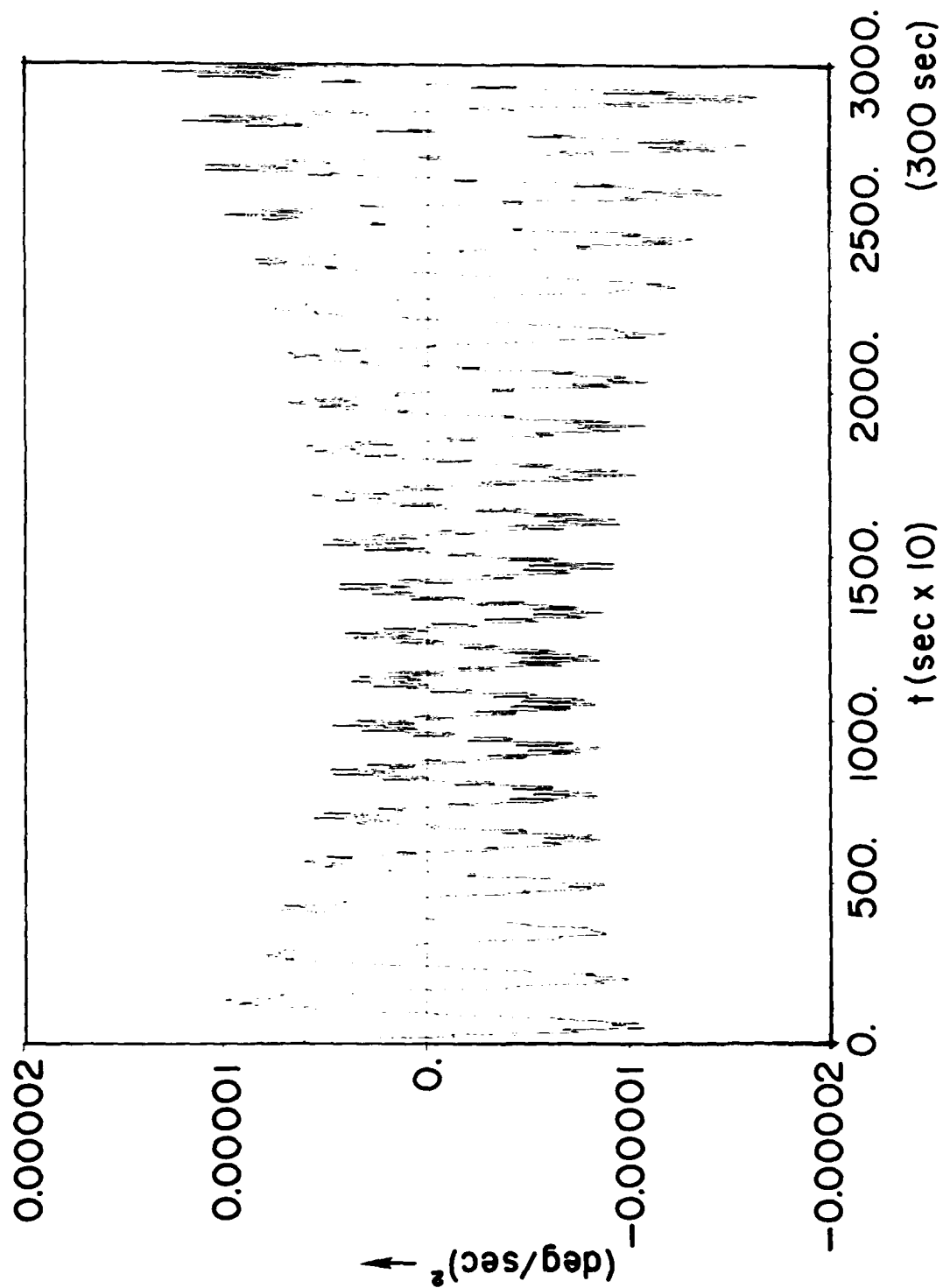


Figure 11. Cross-correlation of X and Y Gyro Data

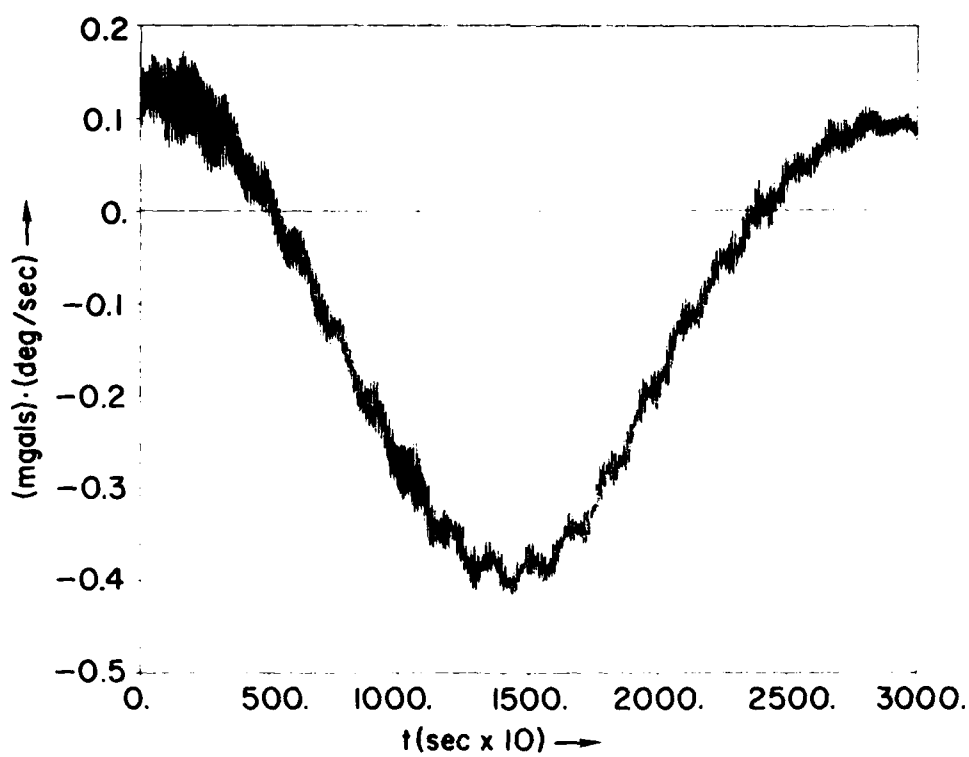
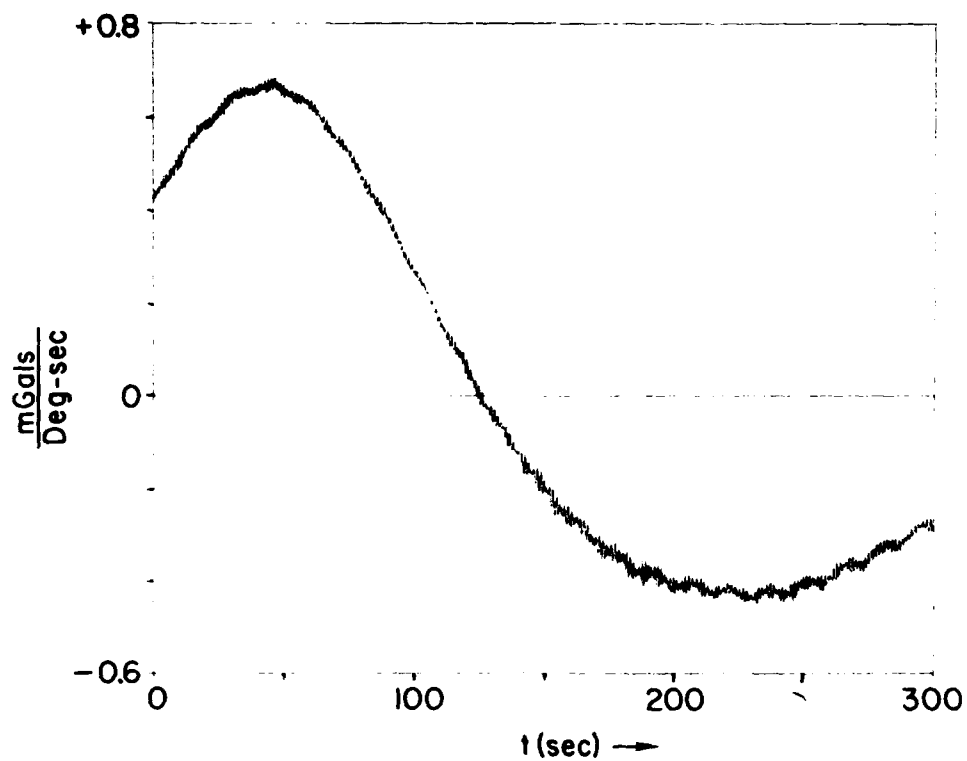


Figure 12a & 12b. Cross-correlation of the VSA With the X and the Y Gyro Data

4.4 Data Processing

The final data array was formed as the point-by-point difference of the VSA output array minus the GPS & Model Array (Figure 13a and 13b). The latter is computed gravity using the current upward continuation model, computed for the position, altitude, vertical axis acceleration, and velocity (to adjust for EOTVOS effect) as given from GPS data. Both arrays are 2043 points in length, samples at a 1-Hz rate, from 17:18 to 17:52 Zulu, both displaying the characteristic 5-minute oscillations arising from balloon dynamics. Due to the effects of a feedback loop in the calculations which generated the GPS and Model Array, a slight time lag was introduced relative to the VSA array; consequently the 5-minute oscillation is also present in the Difference array (Figure 14), at about 10 percent of the amplitude of the two parent arrays. Therefore, the first step in the data reduction process was to offset the two arrays in time by an appropriate amount to eliminate this residual sinusoid. The size of the offset was determined by performing a cross-correlation of the parent arrays; it was found that the cross-correlation function peaked with a three point (3 second) left shift of the GPS & Model array relative to the VSA array. Applying this 3-second offset and re-generating the Difference array (Figure 15) showed a virtual absence of the 5-minute oscillations.

After eliminating the oscillation effect, the next problem was that of spikes in the data. The spikyness of Figures 14 and 15 can be traced directly to the VSA array (Figure 13), having originated in a defective grounding wire in the VSA electronics. A spike-removal algorithm had been developed to address this problem, and was used with moderate success to clean up the data at this stage. The algorithm has two user-selectable parameters: (1) Some multiple of the "local" standard deviation must be set as a threshold for declaring whether spikes are present, and (2) the number of neighboring points to both sides of a declared spike to be removed along with the spike must be input, since spikes often appear as a cluster with leading and trailing sub-threshold noise.

The first level of spike removal is shown in Figure 16, in which parameter (1) was set at 7, parameter (2) at 2. As can be seen in comparing with Figure 15, the two largest spikes were removed, but several smaller ones remained. Several sets of values of (1) and (2) were tried, to get the best compromise between maximum spike removal and minimal effect on good data. The "best" parameter values appeared to be 3.5 for (1), leaving (2) at 2. The result is shown in Figure 17, with the three largest spike clusters of Figure 16 removed.

A final state of data processing was the inclusion of smoothing. The smoother was a symmetric seven-point linear ramp window, applied to each of the available data points; the output from one pass through the smoother is shown on Figure 18, and the output from twenty passes is on Figure 19.

The motivation for data smoothing was to gauge what effect this would have on the mean and variance of the array; most importantly, to check for the persistence of a small bias or trend in the data. Figures 20 and 21 show the change in mean and variance with successive passes through the smoother, going from zero to twenty passes. Figure 20 shows the mean rapidly decreasing from 0.429 mGals with no smoothing to 0.101 mGals after three passes, stabilizing at about -0.02 mGals from thirteen passes on; Figure 21 shows that the variance decreases very sharply, from 11357 mGal² with no smoothing to 1931 mGal² after three passes, then a very gradual reduction to 1084 mGal² after twenty passes. This kind of response to smoothing is characteristic of white noise having a very small, or zero, bias.

Other operations performed on the Difference array involved separating it into sub-arrays, examining the statistics of the sub-arrays for different levels of division, and generating least-squares fits to the total array and to the sub-arrays. The results of these operations are discussed in the next section on data analysis.

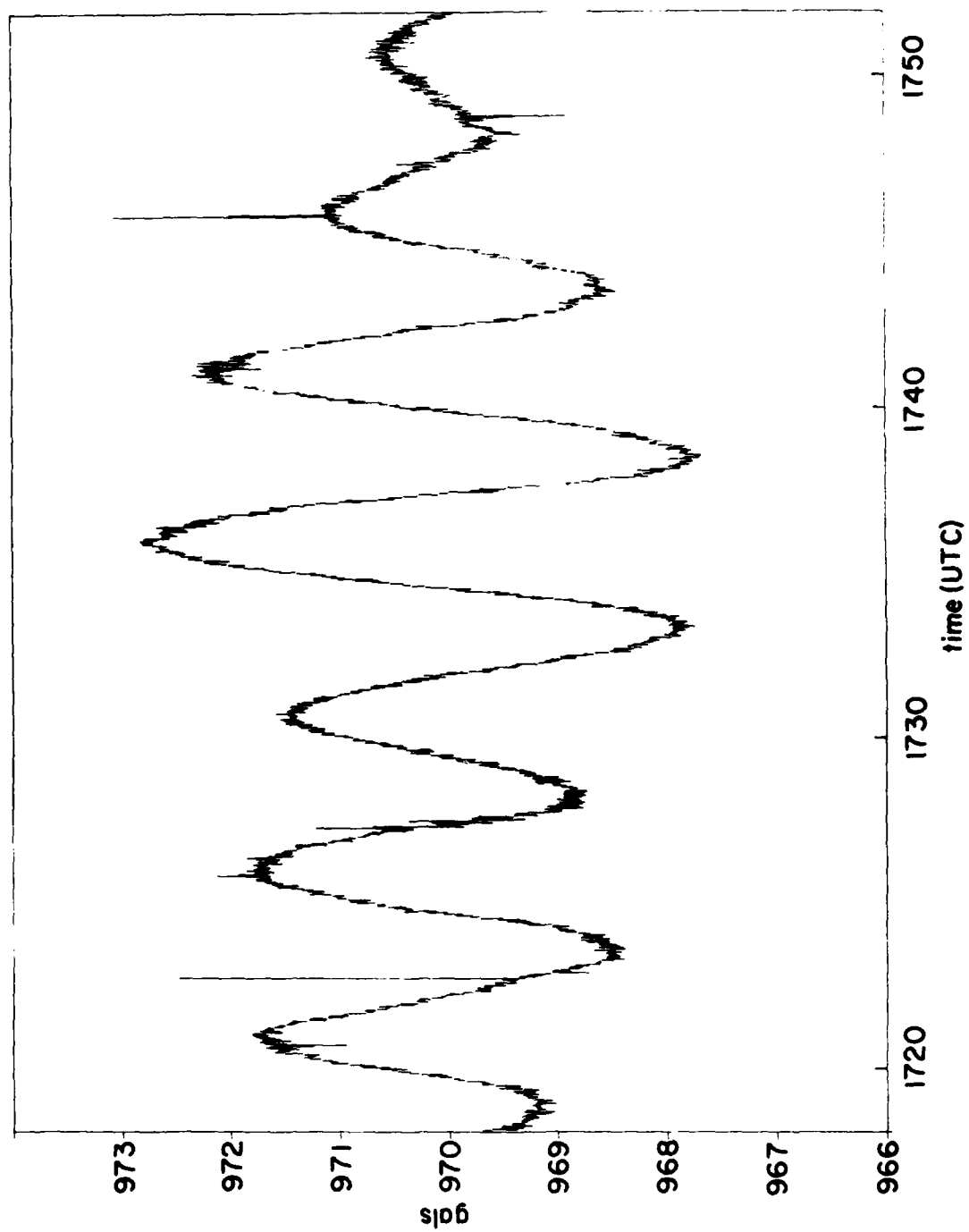


Figure 13a & 13b. VSA Gravity Data Compared With the Modeled Data Based on GPS Tracking Data

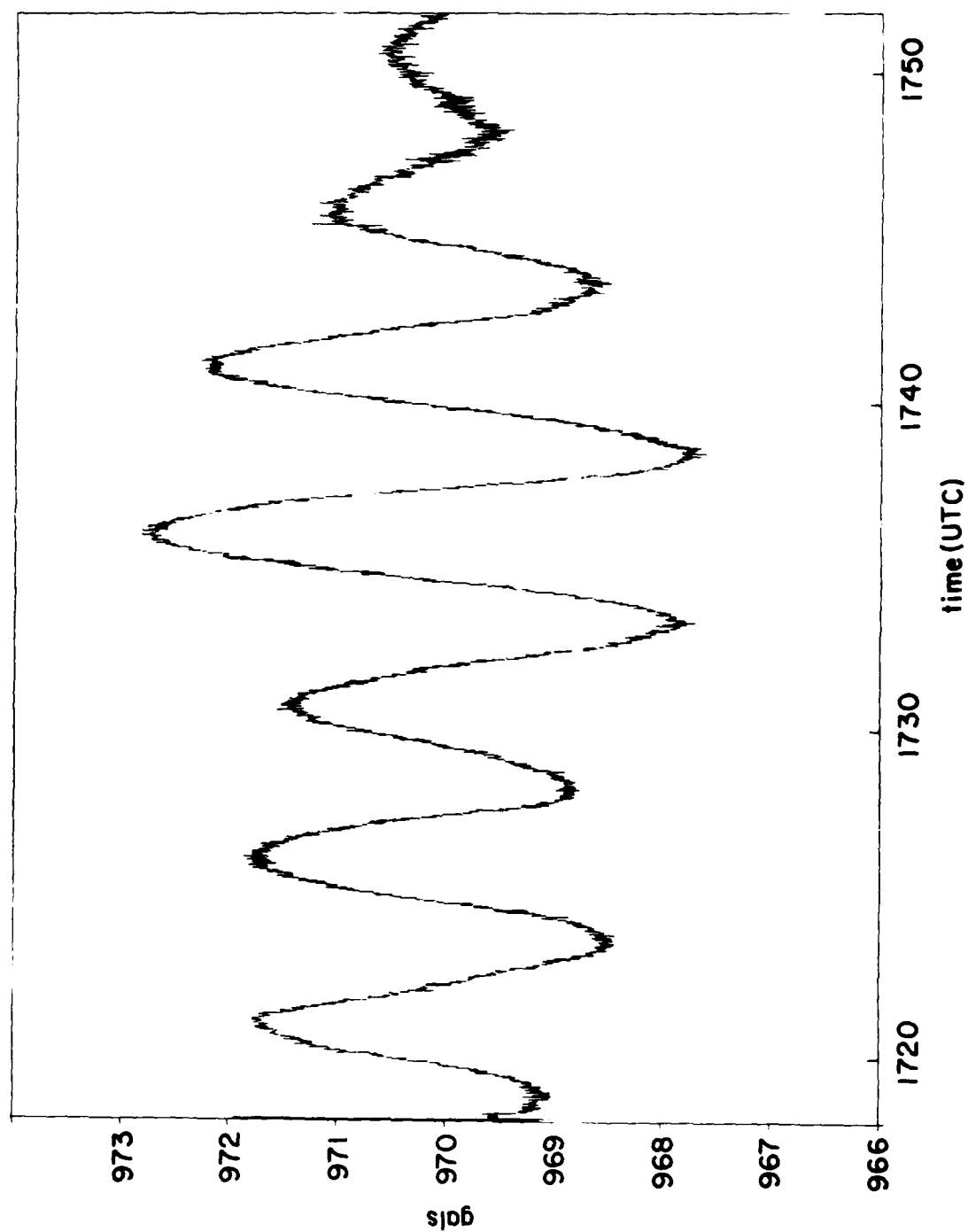


Figure 13a & 13b. VSA Gravity Data Compared With the Modeled Data Based on GPS Tracking Data (Contd)

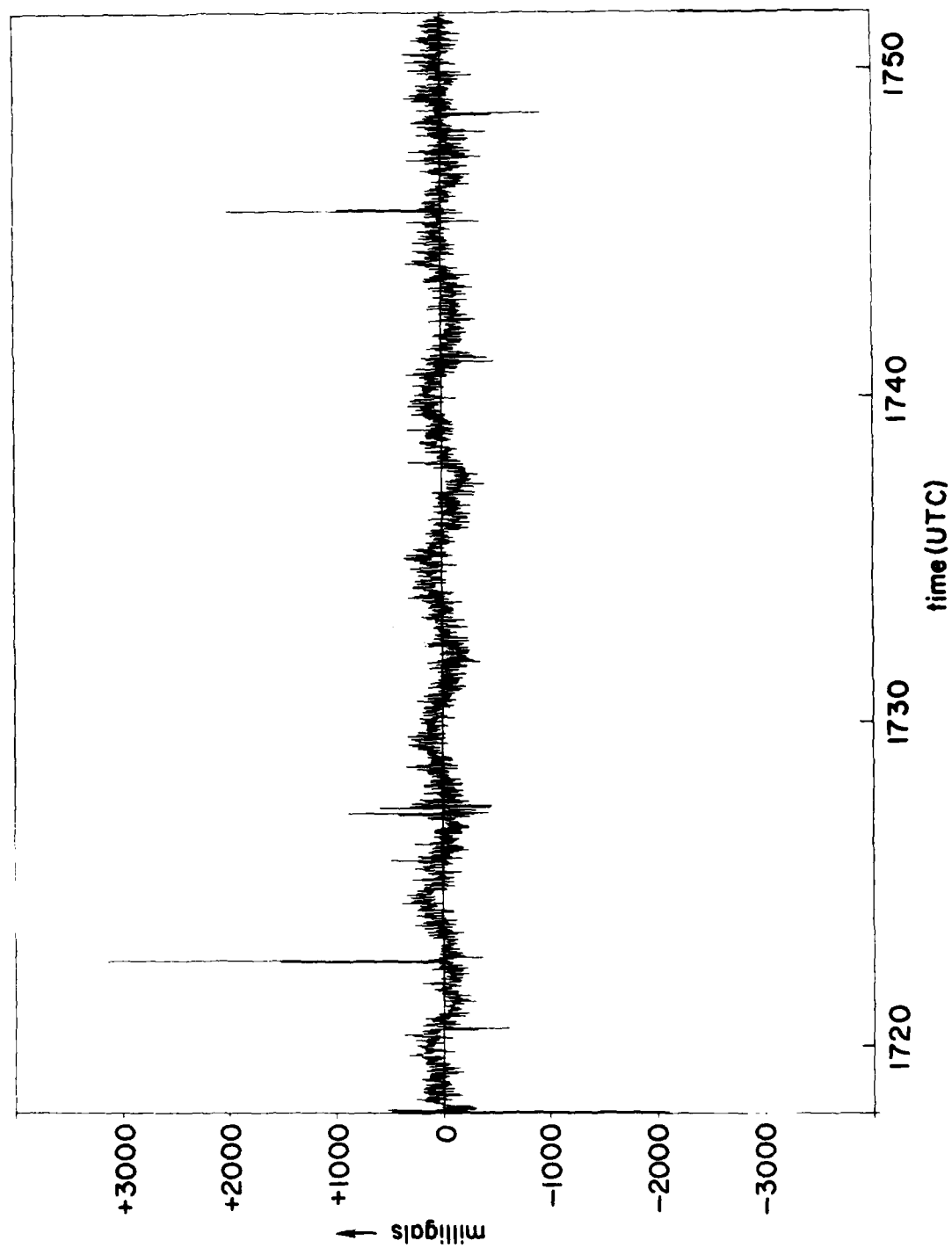


Figure 14. The Difference of VSA Minus Model Gravity Data

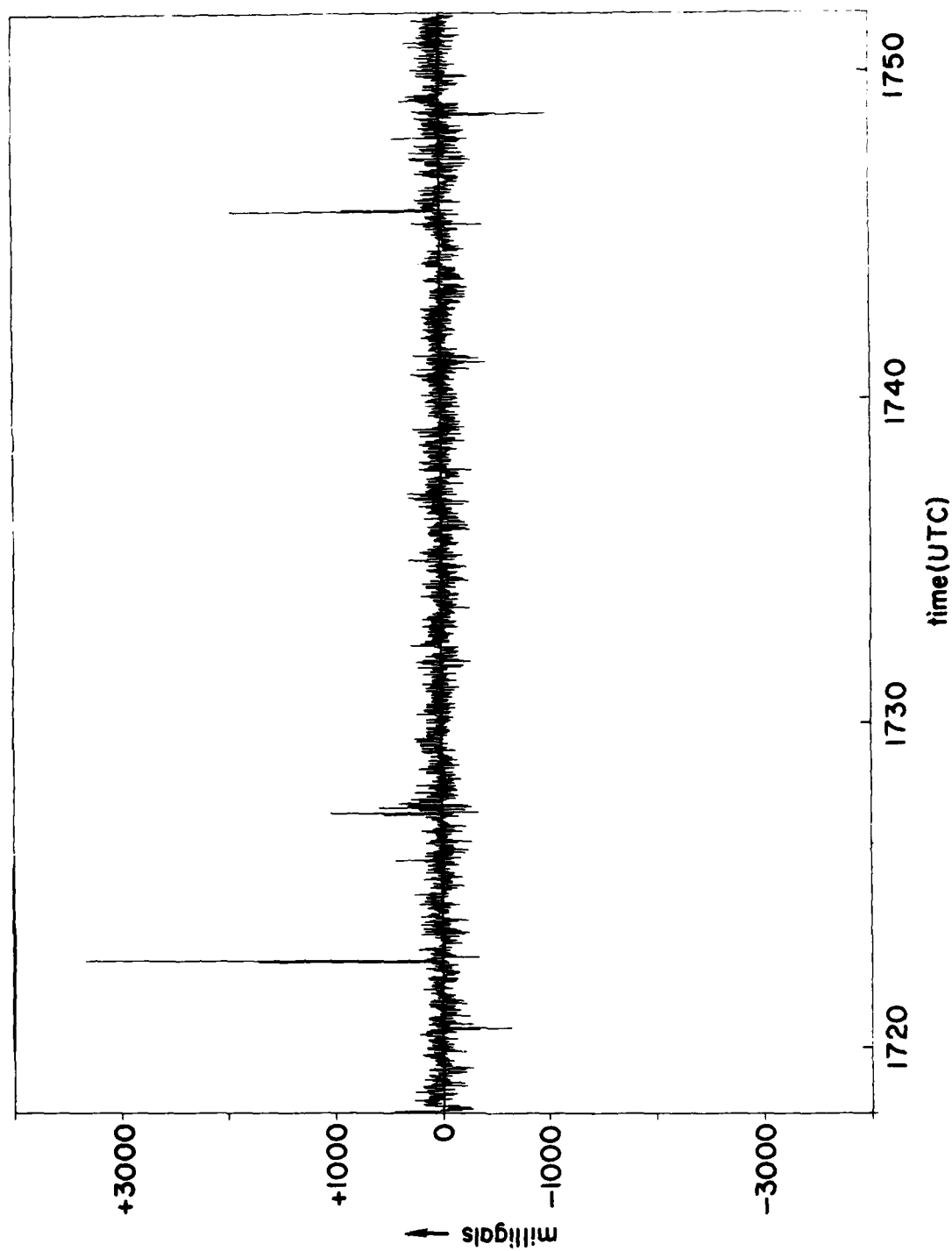


Figure 15. The Difference of VSA Minus Model Gravity Data With the VSA Being Delayed by 3 Seconds.
Note the oscillations evident in Figure 14 are eliminated

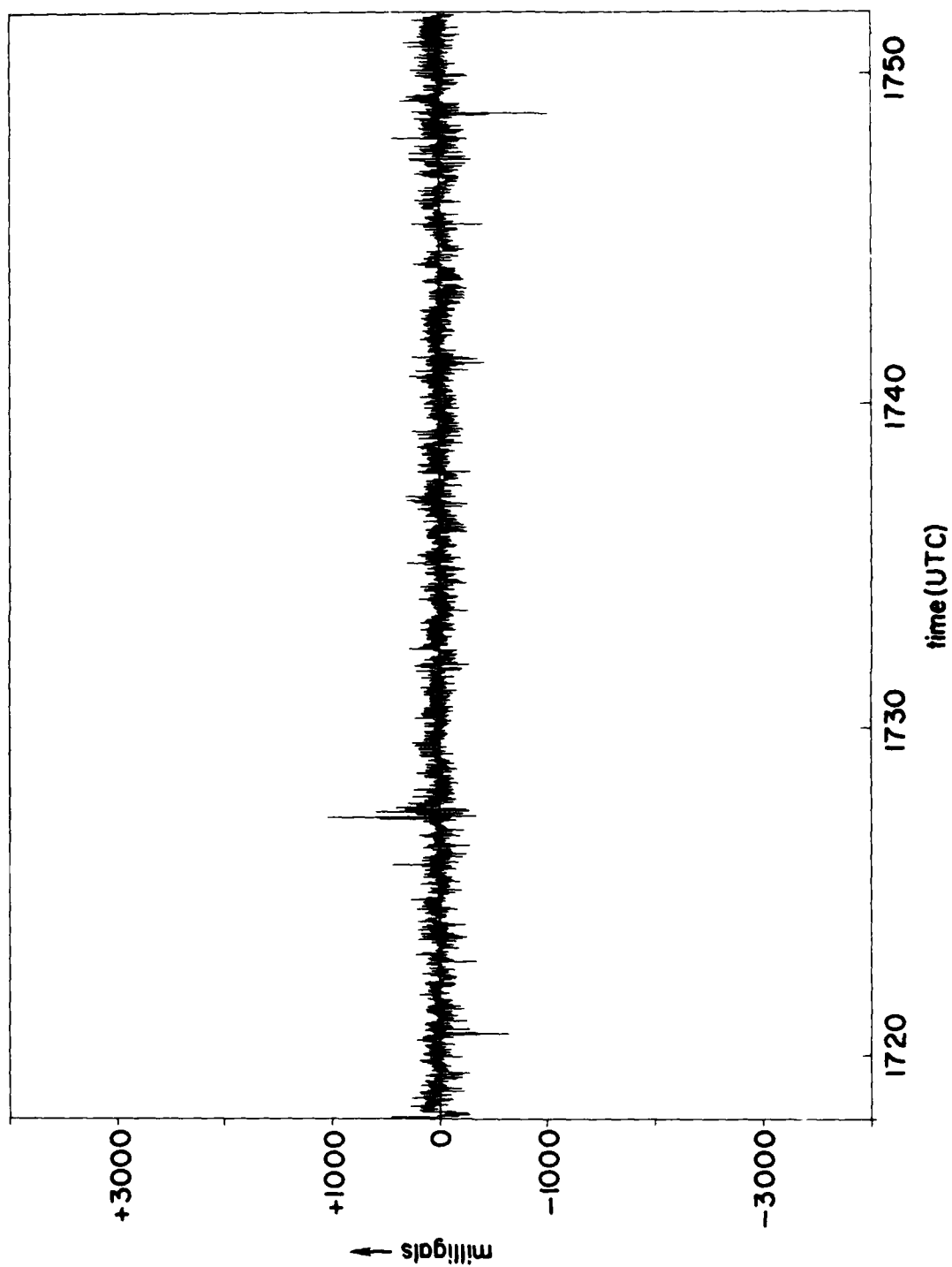


Figure 16. Differenced Data From Figure 15 With the First Level of Spike Removal

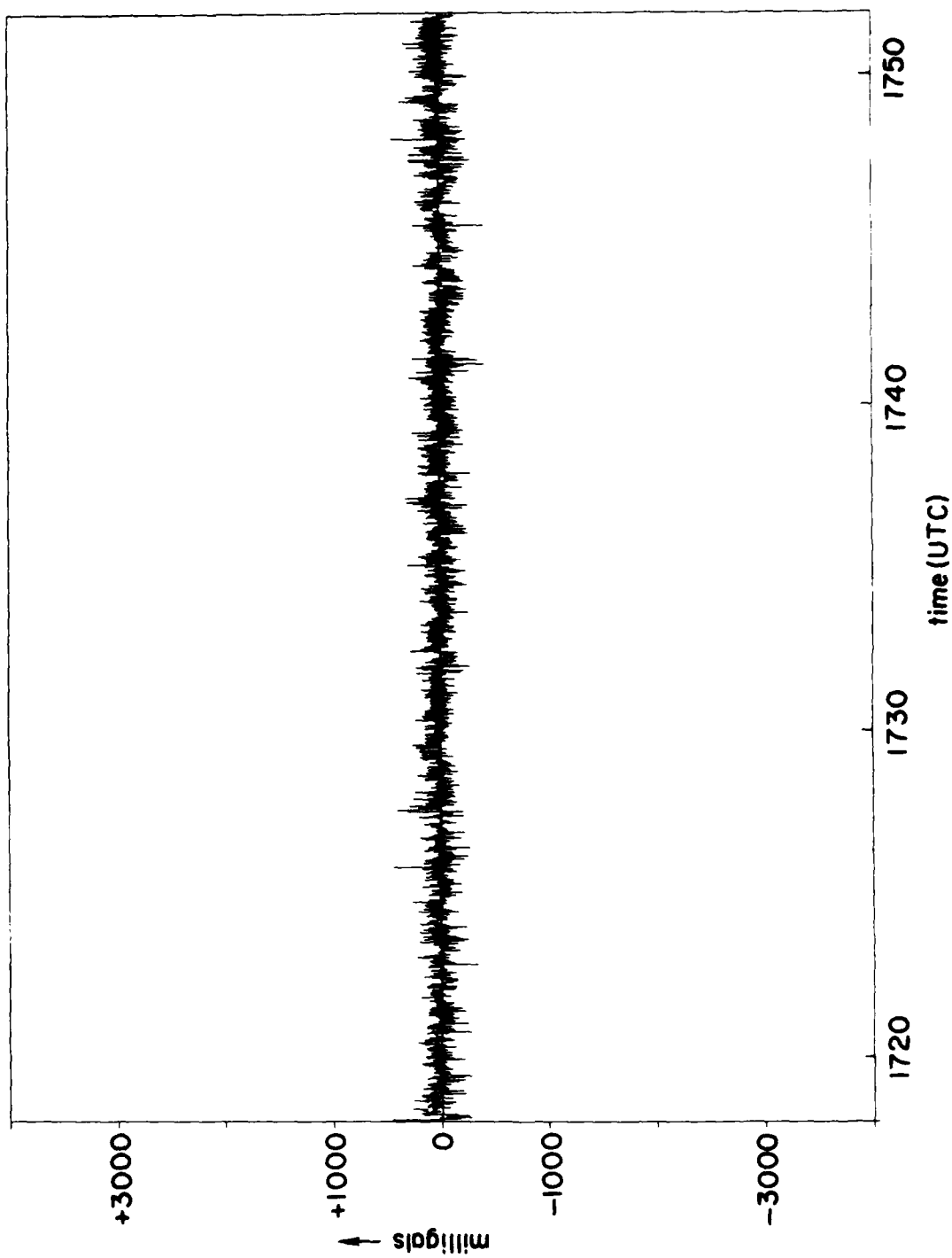


Figure 17. Differenced Data from Figure 15 With the Second Level of Spike Removal

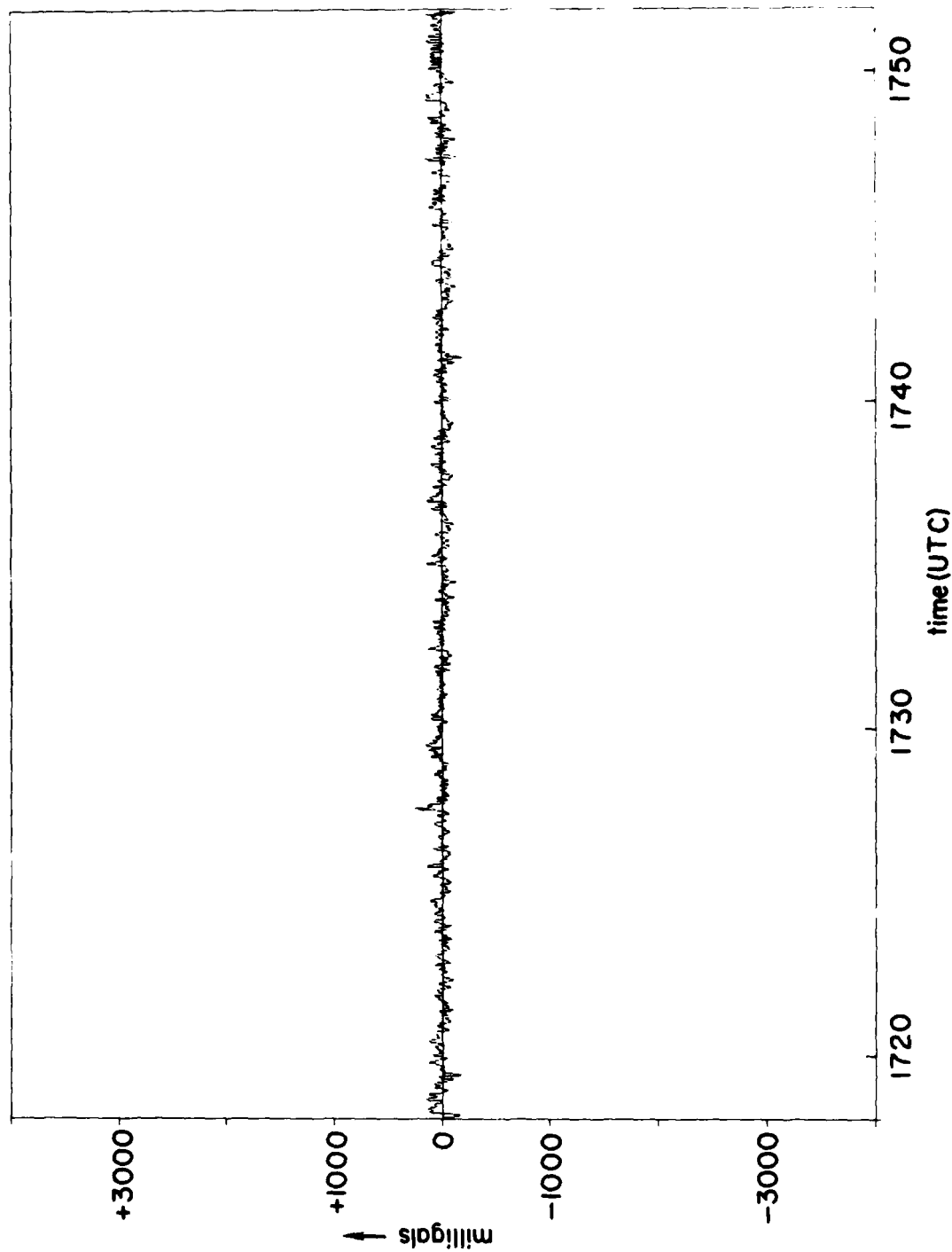


Figure 18. Differenced Data From Figure 15 With the Second Level of Spike Removal and Smoothed in One Pass

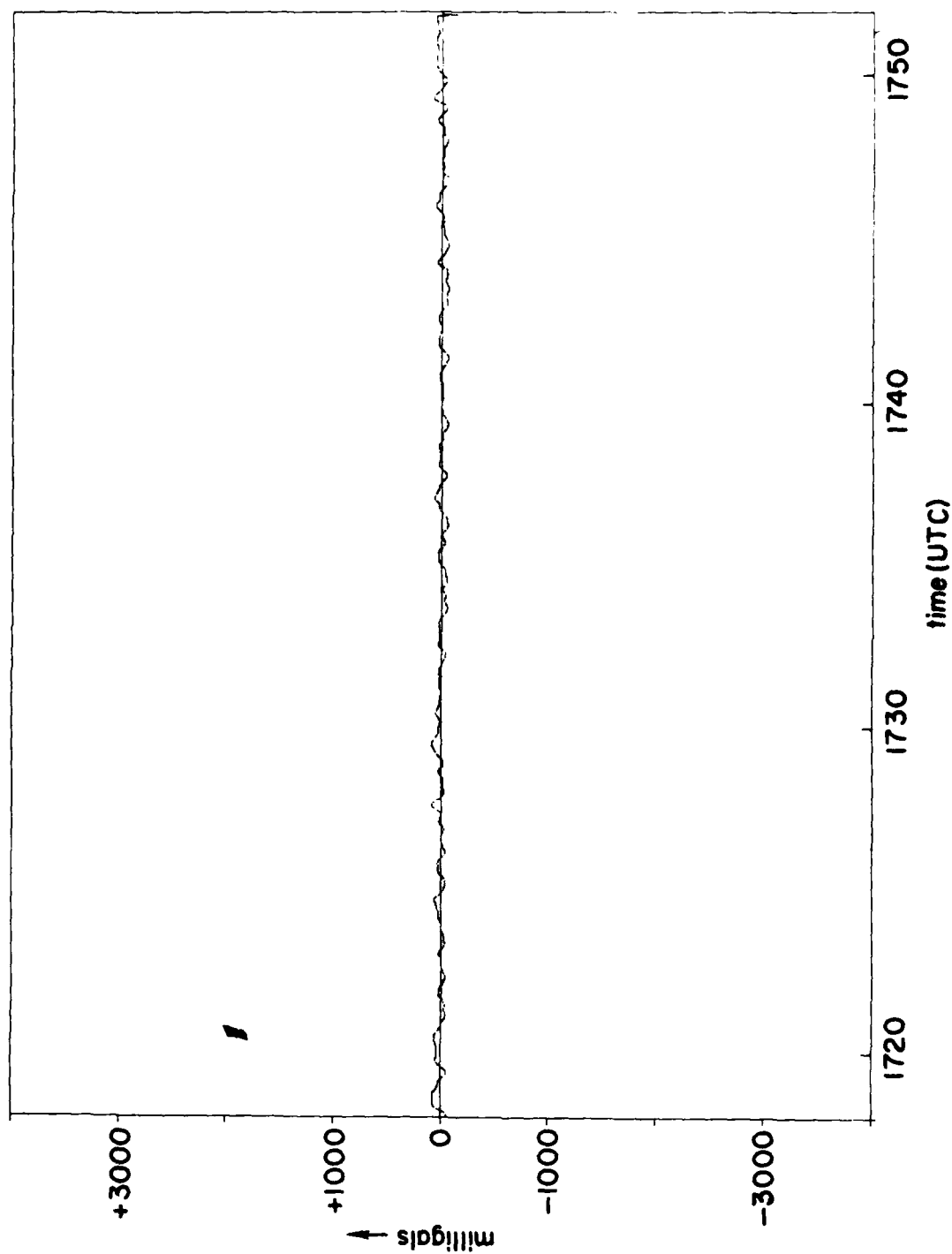


Figure 19. Differenced Data From Figure 15 With the Second Level of Spike Removal and Smoothed in Twenty Passes

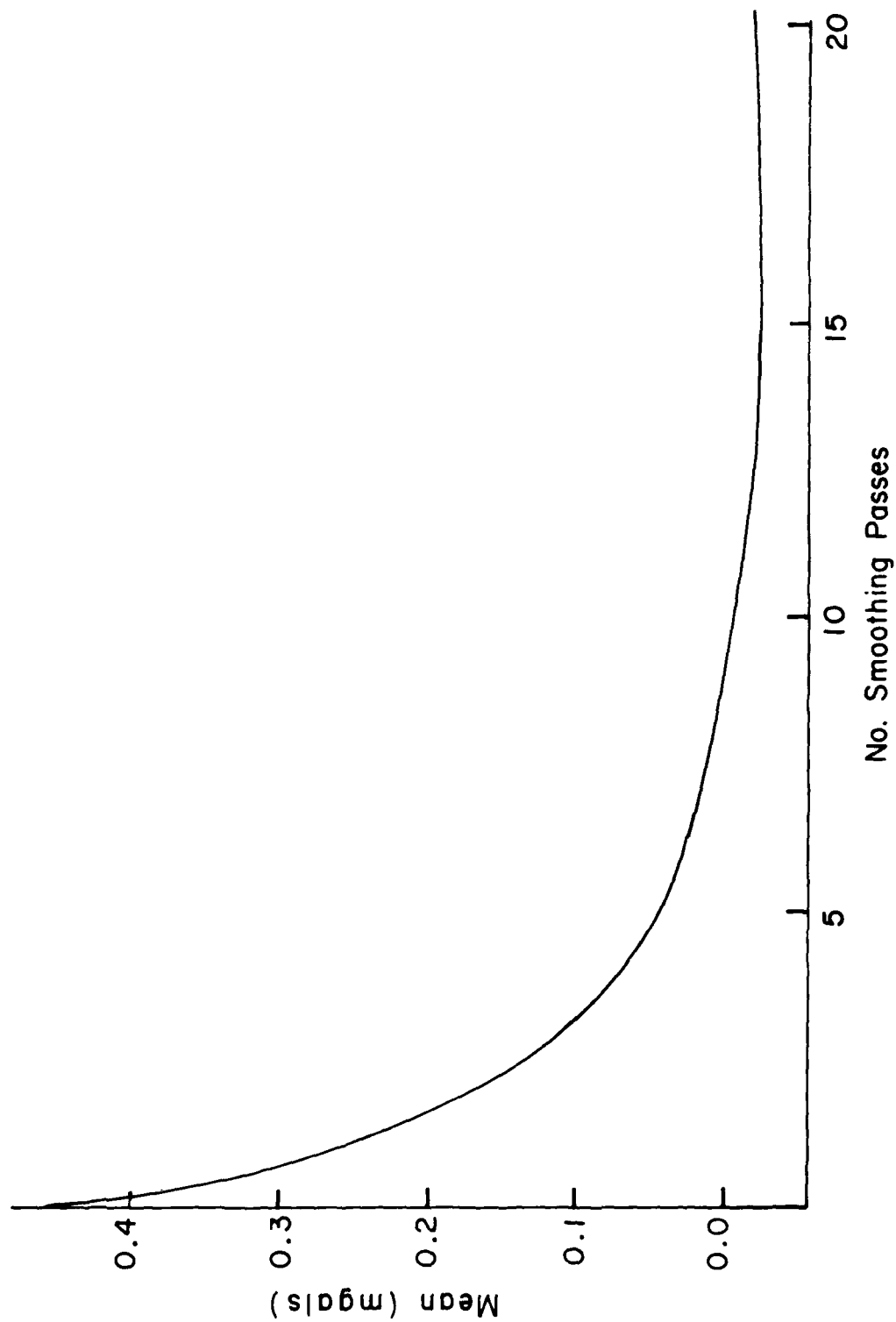


Figure 20. Mean of Difference Array vs Number of Smoothing Passes

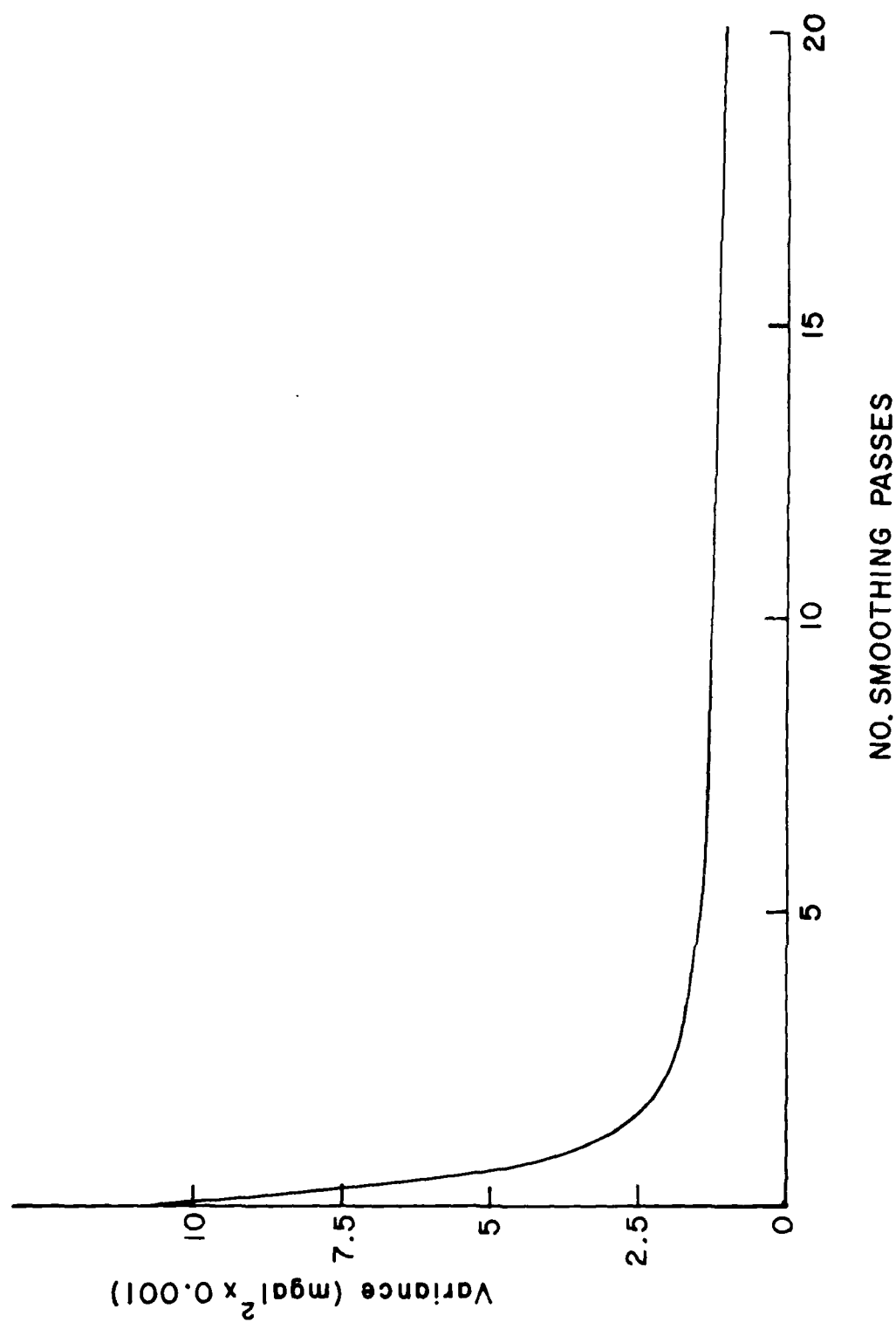


Figure 21. Variance of Difference Array vs Number of Smoothing Passes

4.5 Data Analysis

4.5.1 QUICK LOOK

Testing the data for consistency among channels, timing and precision can be quickly done using GPS tracking, VSA measurements and an AFGL gravity model. GPS positions are used as input for the gravity model and centrifugal acceleration; GPS velocities (East and North) for computing Eotvos corrections; and GPS vertical acceleration for estimates of vertical kinematic accelerations. If there were no misalignments, cross-talk among channels, nor experimental errors, this information would be sufficient for accurate gravity measurements. However, since all these errors obviously do exist, analysis of these data alone can only be used for a "Quick Look".

A quick look at the data is shown in Figure 22. The GPS gravity model is computed from GPS geodetic position, so the two should track well. The GPS + model is the mathematical estimate of measured gravitational acceleration based on GPS tracking; these data are compared with the raw VSA measurements. The last plot is the difference of the two. Notice the cyclical oscillation of about 0.08 hours (5 minutes) with an amplitude of about 200 mGals. If we advance the GPS data by 3 seconds, or retard the VSA data by 3 seconds, this oscillation goes away. It is possible that the processing and filtering of the GPS data delayed it by some time. Nevertheless, after this time shift, the rms noise drops to about 20 mGals. Probably the single biggest contribution to this noise is the faulty ground wire in the VSA, which unfortunately, cannot be corrected.

Overall, if this quick look shows the data to be good to 20 mGals, or even 200 mGals (including the 5-minute period), we conclude the instruments work very well, and a proper treatment including all the available data should reduce the uncertainties by a significant amount; an order of magnitude improvement would not be unreasonable.

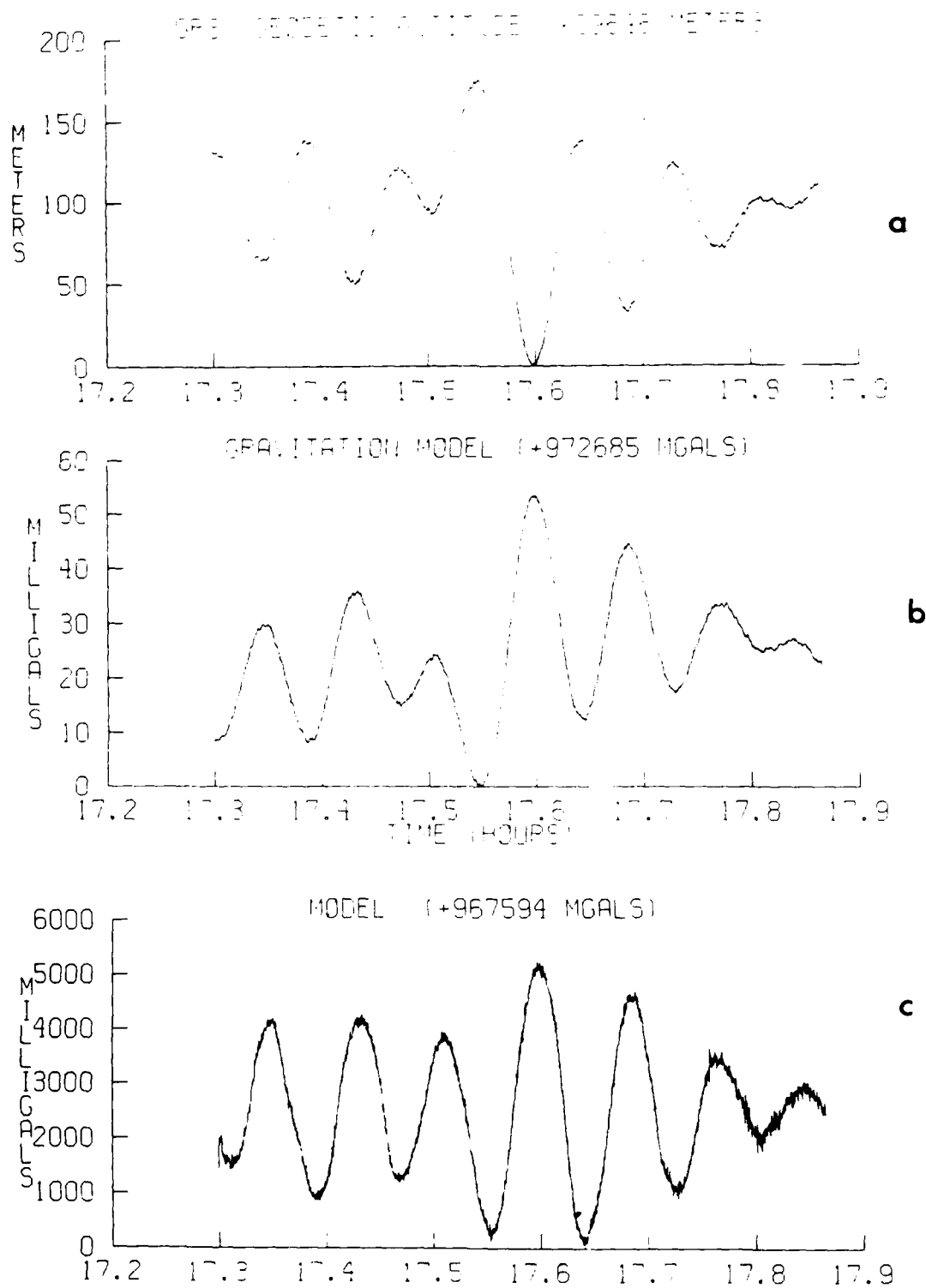


Figure 22. Quick Look at About 35 Minutes of Data: (a) GPS Geodetic Altitude; (b) Gravitation Model Based on GPS Positions; and (c) Gravity Model Based on GPS Tracking of Position, Velocity and Acceleration

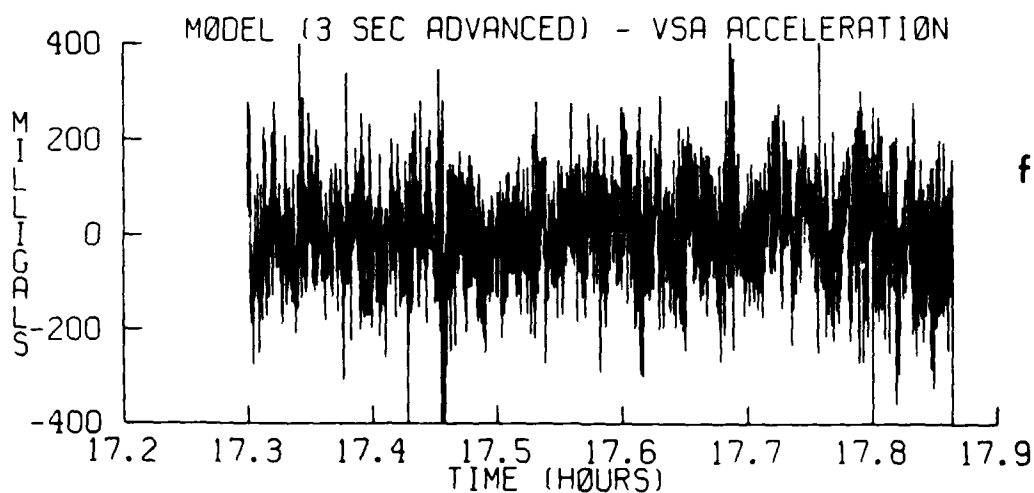
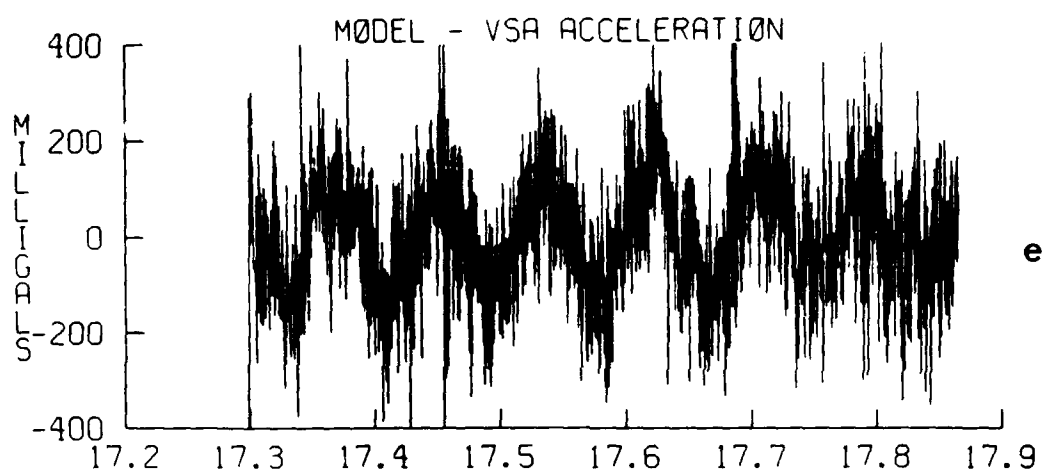
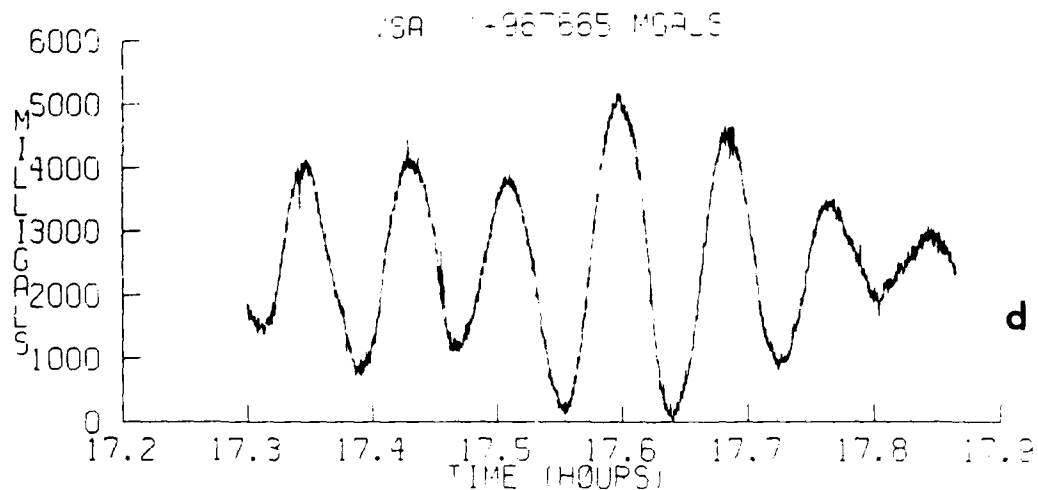


Figure 22. Quick Look at About 35 Minutes of Data: (d) Gravity as Measured by the VSA; (e) Gravity Model Minus VSA; and (f) Gravity Model Minus VSA With the Model Being Advanced by 3 Seconds (Contd)

4.5.2 DETAILED LOOK

Several statistical tests were performed on the data, in an attempt to form an accurate perception of what was the physical significance, if any, behind the numbers. In simply looking at the data with sinosoid and spikes removed, several conclusions could be drawn regarding the Difference array: (1) The mean of the array was extremely small (0.429 milligal), from both the measurement accuracy arguments and the scatter, or variance, in the data; (2) no linear trend was noticeable; and (3) fluctuations, or noise, in the data seemed to be fairly uniform and constant.

These preliminary conclusions beg for underlying answers: Is the mean value to be accepted as is? Is the data acceptable with this level of noise? Is there any trend in the data, but too small to notice on first inspection?

The first question was motivated by the fact that the standard deviation is about 106 milligals, both for the full array and any subarray, that is, the noise is very uniform and homogeneous throughout. If all the statistics were this uniform, then it would be reasonable to assume that measurements of the mean on subsets of the array should be "fairly close" to the total mean of 0.429 milligals, with "fairly close" quantitatively undefined. As it turns out, the scatter in the mean is much larger than 0.4 milligals, as Table 1 shows.

Table 1. Data Points Used for Statistical Test 1

Data Points Included	Mean (mGal)	Standard Deviation (mGal)
1-2033 (Entire Array)	0.4289	106.57
40-1979	-1.6773	104.80
70-1969	-2.7590	104.34
1-1016 (First Half)	6.7922	101.01
1017-2032 (Second Half)	-5.8484	111.51
1-508 (First Quarter)	8.4309	105.38
1017-1525 (Third Quarter)	-8.2163	106.64

The point the above data make is that the proximity of $\mu = 0.429$ mGal to zero is really a fortuitous coincidence; changing the array size from 2033 to 1940 points, a 4.6 percent reduction, changes μ by almost a factor of 5, or 400 percent. The average deviation of the first and second half means from zero, 6.3203, is almost 15 times the deviation from zero of the full array mean. Meanwhile, the standard deviation value fluctuates very little, being in the range of 106 ± 6 mGals for all subsets measured. Another way of illustrating this point is to subdivide the array into halves, then quarters, and so on, and examine the scatter, or 1 sigma value, for the average of the subsets' means and the average of the subsets' 1 sigma values, or standard deviations. This is tabulated below as Table 2; the last column is the values of $\sigma/(1/2\sqrt{N})$, where σ is the average standard deviation for that row and N is the subarray size for that row. A fairly simple physical argument would show that the 1 sigma of the average of the subarrays' means should approximate this value, if the data is normally distributed.

Table 2. Data Points Used for Statistical Test 2

Subset Size	Standard Deviation of μ 's	Standard Deviation of σ 's	$\sigma/(1/2\sqrt{N})$
Half (1016 pts)	8.983	7.425	6.647
Quarter (508)	7.667	8.061	9.407
Eighth (254)	15.442	8.657	13.302
Sixteenth (127)	18.405	11.086	18.812

Thus, the scatter in the mean value of the Difference array behaves similarly to independent Gaussian noise. For $N \approx 2032$, $\sigma/(1/2\sqrt{N}) = 4.70$; therefore, the proper conclusion to be drawn from the statistics of the available data is that, due to the high level of stochastic noise originating in the VSA, the measured mean lies within a range of approximately ± 5 milligals of zero. That the measured mean of the full array is less than half a milligal is only a statistical result, albeit fortuitous. Inasmuch as this does not seem as impressive as declaring a mean of 0.429 mGal, the bounds of $(-5, +5)$ is significant in that, with a noisy gravimeter and only 34 minutes of useful observation time, the measured value of g is within 5 ppm of the modelled value.

One last aspect of the data analysis is the matter of the presence or absence of a linear trend. To examine the data for possible trends, the computer code performed a least-squares fit to a straight line with the Difference array, both for the full array and for subarrays down to one-sixteenth size. For the full array, the least-squares fit gave a slope of -0.00975 mGals/data point; for the smallest subarrays, the average slope is -0.03479 ± 0.3432 mGals/data point. A histogram plot of the slope and mean of each of the sixteen subarrays is shown on Figure 23, and appears to support the presence of a quadratic trend in the means and a linear trend in the slopes, as shown by the dashed lines. A least-squares fit to the histogram of slopes yields a straight line having a slope of $+0.0420$ mGals/data point/subarray and a y-intercept (left edge) of -0.392 mGals/data point.

Although the evidence might be persuasive, it is very problematical whether this trend is genuine or merely of statistical origin. The human mind will automatically look for patterns, and that may be the case here. On the other hand, any one of several effects could give rise to a trend of this type: there could be a scale factor drift in the VSA due to temperature changes or some other environmental effect, there could be a gradual error accumulation in the GPS & Model channel, or some other unforeseen effect could be affecting the Difference array values. The most likely source is judged to be statistical - the scatter in the data have been arranged, through chance, to mimic a pattern with no underlying cause. At any rate, it would be speculation to form any conclusions regarding the plots of Figure 23, the current state of Ducky II data shows the need for additional balloon flights with an improved low-noise-level gravimeter and the acquisition of usable data sets much larger than the 33.9 minutes made available on this flight. A gravimeter with an integration, or smoothing, window of about 10 seconds should drop the instrument noise level down to one or two milligals; that plus several hours of observation time would allow for vastly improved measurements.

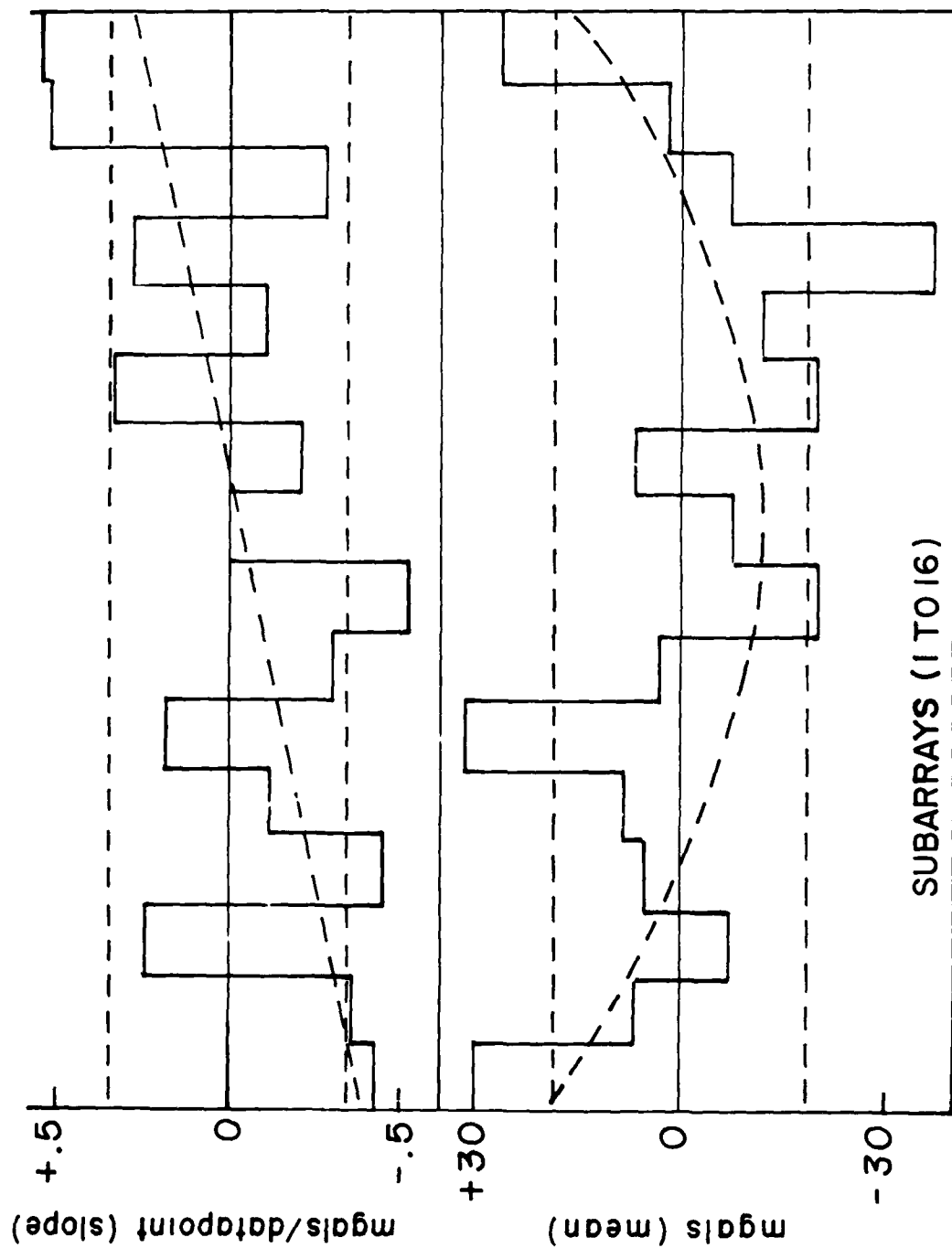


Figure 23. Slopes and Means of Subarrays 1 to 16. This plot shows the differences between the model and VSA in short segments of time to see effect of using long or short time segments

References

1. Bowin, C.O., Wing, C.G., and Aldrich, T.C. (1969) Test of the MIT vibrating string gravimeter, J. Geophys. Res. 74, 12:3278-3280.
2. Bowin, C.O., Folinsbee, A., and Aldrich, T.C. (1970) Test of digital VSA sea gravity meter and comparison with LaCoste and Romberg gyro stabilized gravity meter (Abstract), Trans. Am. Geophys. Union 51, 4:261.
3. Bowin, C., Aldrich, T.C., and Folinsbee, R.A. (1972) VSA gravity meter system: tests and recent developments, J. Geophys. Res. 77:2018-2033.
4. Lazarewicz, A.R., Schilinski, B.J., Cowie, R.J., Rice, C.L., Moss, P., and Carter, L.N. (1985) Balloon-Borne, High-Altitude Gravimetry, The Flight of DUCKY IA (October 1983), AFGL-TR-85-0342, ADA 169942.
5. DeLeeuw, J.H., and Kung, W.L. (1984) Development of motion-sensing package for high-altitude balloons, University of Toronto Institute for Aerospace Studies, AFGL-TR-85-0258, ADA 170225.
6. Iliff, R.L., and Sands, R.W. (1984) Relative Gravity Measurements at Holloman AFB, New Mexico, AFGL Technical Memorandum Series 95.
7. Iliff, R., and Sands, R.L. (1983) The AFGL Absolute Gravity Measuring System, A Final Report and Operating/Maintenance Manual, AFGL-TR-83-0297, ADA 147853.
8. Marson, I., and Alasia, F. (1980) Absolute Gravity Measurements in the United States of America, AFGL-TR-81-0052, ADA 099017.
9. Zumberge, M.A., Fowler, J.E., and Gschwind, J. (1983) Results from an absolute gravity survey in the United States, J. Geophys. Res. 88(No. B9).

LIST OF ACRONYMS

AFGL	Air Force Geophysics Laboratory
ARL	Applied Research Laboratories, University of Texas.
CIGTF	Central Inertial Guidance and Testing Facility
CIRIS	Completely Integrated Range Instrumentation System
DMA	Defense Mapping Agency
FM	Frequency Modulation
GPS	Global Positioning System
I*S*P	Interactive Signal Processing (Bedford Research Associates)
MSL	Mean Sea Level
NSWC	Naval Surface Weapons Center
OSU	Ohio State University
PCM	Pulse-Code Modulation
PSL	Physical Sciences Laboratory, New Mexico State University
UTIAS	University of Toronto Institute for Aerospace Studies
VSA	Vibrating String Accelerometer (gravimeter)
WSMR	White Sands Missile Range
WHOI	Woods Hole Oceanographic Institute
Z-100	Zenith Z-100 microcomputer system

Appendix A

Relative Gravity Measurements at Holloman AFB, NM

Note: This appendix is taken verbatim from AFGL Technical Memorandum Series 95.⁶ It is included here for completeness.

Relative-gravity measurements were made at selected sites at Holloman AFB, NM,⁶ in support of the AFGL balloon-borne gravity experiment. The site locations, chosen in accordance with the experiment requirements, were:

(1) The Advanced Inertial Test Laboratory (AITL), Building 1256: This is an absolute site measured by AFGL/LWG in 1980,⁷ the Istituto di Metrologia "G. Colonnetti" (IMGC) Italy in 1980,⁸ and the Joint Institute for Laboratory Astrophysics (JILA) in 1982.⁹ The absolute gravity marker in Room 10 in the AITL building was the starting and closing site for all measurements.

(2) The High Bay, Building 850: The experiment package assembly, testing, and instrument calibration were performed in the High Bay.

6. Iliff, R.L., and Sands, R.W. (1984) Relative Gravity Measurements at Holloman AFB, New Mexico, AFGL Technical Memorandum Series 95.

7. Iliff, R., and Sands, R.L. (1983) The AFGL Absolute Gravity Measuring System, A Final Report and Operating/Maintenance Manual, AFGL-TR-83-0297, ADA 147853.

8. Marson, I., and Alasia, F. (1980) Absolute Gravity Measurements in the United States of America, AFGL-TR-81-0052, ADA 099017.

9. Zumberge, M.A., Fowler, J.E., and Gschwind, J. (1983) Results from an absolute gravity survey in the United States, J. Geophys. Res. 88(No. B9).

(3) The Altitude Test Chamber, Building 1261: Calibration data were taken here during high-altitude simulation tests.

(4) Secondary Test Chamber, Building 1261: Due to a malfunction in the main test chamber, a secondary high-altitude simulation chamber was used for a portion of the tests. The floor of the secondary chamber is about 50 cm higher than the floor of the main chamber, so the gravity value is lower. The gravity value in the secondary chamber was calculated using the previously determined gradient of 0.285 mGal/meter.

(5) Nenninger Site, Launch Pad: Measurements were made 30 m diagonally in from each of the four corners, and at the center of the launch pad. Five points were made primarily because of the relatively large gravity differences, approximately one mGal, encountered at the launch pad and the uncertainty of the launch point. Due to wind shifts, the launch point frequently is not known until just before launch.

It should be pointed out that the measurement made at the center is not at the crosspoint of the E-W/N-S reflecting markers embedded in the launch pad. These markers no longer cross at the center, due to additional lengthening of the pad in the north-south direction.

The gravity transfers were made from the AITL building with a LaCoste-Romberg G-120 meter loaned to AFGL by the Geodetic Survey Squadron (GSS). The G meter was set on its leveling feet since no disk was available. Furthermore, the meter was placed in an east-west orientation with the two leveling screws to the east, and the single screw to the west side. Three readings were made at each site and the results were corrected for earth tides, meter factor, and meter drift. Meter drift is based on constant drift from start to closure of readings.

Relative Measurements

The confidence level of the relative measurements is ± 0.15 mGal (except where noted).

(1) AITL (Building 1256) (absolute gravity site):	979139.600 \pm 0.009 mGal
(2) High Bay (Building 850):	979136.002 mGal
(3) Test Chamber (Building 1261):	979136.536 mGal
(4) Secondary Test Chamber:	979136.393 \pm 0.50 mGal
(5) Nenninger Site (Launch Pad):	
a. Southeast Corner:	979140.708 mGal
b. Northwest Corner:	979141.782 mGal
c. Southwest Corner:	979141.132 mGal
d. Northeast Corner:	979141.286 mGal
e. Center of Pad:	979141.236 mGal

Appendix B

Science and Balloon-Control Data Stream

Word No.	ADC Chann. No.	ADC Precision	Description
1			ASC II-DLE - Beginning of Message Header
2			ASC II - STX
3			ASC II Character, most sig.
4			" " -GPS Pulse I.D.: 6
5			" " characters sent most-
6			" " to-least significant.
7			" " Describe time in GSP
8			" " second of week
9			ASC II Character, least sig.
10			Binary, -Count value (0-9)
11			Two BCD Characters, least sig. -VSA data: 8
12			" " " BCD digits
13			" " " , most sig.
14	0	(12)	Binary, LSB - VSA Inner Oven Control Voltage
15			" , MSB
16	1	(12)	" , LSB - VSA Outer Oven Control Voltage
17			" , MSB
18	2	(12)	" , LSB - Magnetic Compass Heading
19			" , MSB
20	3	(12)	" , LSB - Motion Sensor Box Temp.
21			" , MSB
22	4	(12)	" , LSB - X-Gyro low gain
23			" , MSB

Word No.	ADC Chann. No.	ADC Precision	Description	
24	5	(12)	Binary, LSB	- Y-Gyro low gain
25			, MSB	
26	6	(12)	" , LSB	- Z-Gyro low gain
27			, MSB	
28	7	(12)	" , LSB	- X-Gyro high gain
29			, MSB	
30	8	(12)	" , LSB	- Y-Gyro high gain
31			, MSB	
32	9	(12)	" , LSB	- Z-Gyro high gain
33			, MSB	
34	10	(12)	" , LSB	- X Accelerometer low gain
35			, MSB	
36	11	(12)	" , LSB	- Y Accelerometer low gain
37			, MSB	
38	12	(12)	" , LSB	- Z Accelerometer low gain
39			, MSB	
40	13	(12)	" , LSB	- X Accelerometer high gain
41			, MSB	
42	14	(12)	" , LSB	- Y Accelerometer high gain
43			, MSB	
44	15	(12)	Binary, LSB	- Z Accelerometer high gain
45			, MSB	
46	16	(12)	" , LSB	- X Magnetometer
47			, MSB	
48	17	(12)	" , LSB	- Y Magnetometer
49			, MSB	
50	18	(12)	" , LSB	- Z Magnetometer
51			, MSB	
52	19	(12)	" , LSB	- Pressure Altimeter, 0-15 psi
53			, MSB	
54	20	(12)	" , LSB	- Pressure Altimeter, 0-2.0 psi
55			, MSB	
56	21	(12)	" , LSB	- Pressure Altimeter, 0-0.5 psi
57			, MSB	
58	22	(12)	" , LSB	- Command Verification Monitor
59			, MSB	
60	23	(12)	" , LSB	- Flight Termination Monitor
61			, MSB	
62	24	(8)	Binary	- VSA Pwr. Converter Heat Sink Temp
63	25	(8)	"	- Z80 Card Cage Temp
64	26	(8)	"	- GPS #1 Temp
65	27	(8)	"	- GPS #2 Temp

Word No.	ADC Chann. No.	ADC Precision		Description
66	28	(8)	Binary	- DigiData Tape Unit Temp
67	29	(8)	"	- Up Camera Temp
68	30	(8)	"	- Down Camera Temp
69	31	(8)	"	- C Band Xponder Temp
70	32	(8)	"	- Data Xmitter #1 Temp
71	33	(8)	"	- Data Xmitter #2 Temp
72	34	(8)	"	- Battery Section #1 Temp
73	35	(8)	"	- Battery Section #2 Temp
74	36	(8)	"	- VSA 28V Monitor
75	37	(8)	"	- GPS 28V Monitor
76	38	(8)	"	- Primary 28V Monitor
77	39	(8)	"	- Backup 28V Monitor
78	40	(8)	"	- Primary 12V Monitor
79	41	(8)	"	- Backup 12V Monitor
80	42	(8)	"	- Z80 5V Monitor
81	43	(8)	"	- Pri. Cmd. Rx. Signal Strength
82	44	(8)	"	- Backup Cmd. Rx. Signal Strength
83	45	(8)	"	- VSA Inner Heat Blanket Voltage
84	46	(8)	"	- VSA Outer Heat Blanket Voltage
85			Control	- Digital Monitor #1
86			"	- Digital Monitor #2
87			"	- Digital Monitor #3
88			"	- Digital Monitor #4

Digital Monitor #1 - Switch Indicators , Word No: 85

Bit No:

0	Power Control Indicator for Motion Sensor System
1	Ballast Pour
2	Gas Valve Open
3	Burst Switch Armed
4	Burst Pin pulled above 10K feet
5	Burst Pin pulled below 10K feet
6	Termination by Primary
7	Termination by Backup

Digital Monitor #2 - Command Veritication, Word No: 86

Bit No:

P1 - Pin #

0	LSB	1	, P1-7
1		2	, P1-8
2		4	, P1-9
3		8	, P1-10
4		16	, P1-11
5		32	, P1-12
6	MSB	64	, P1-13
7	Execute Digital Monitor Outputs		, P1-14

Digital Monitor #3 - Flight Termination Timer Status Word No: 87

Bit No:

Timer Pin

0	Status bit 1	, U
1	Status bit 2	, V
2	Status bit 3	, W
3	Status bit 4	, X
4	Status bit 5	, Y
5	Status bit 6	, Z
6	Status bit 7	, a
7	Status bit 8	, b

Digital Monitor #4 - Tape Recorder Status and Back-up Command Verification
Word No: 88

Bit No:

0	Busy (active low)
1	Select (active low)
2	LSB 1
3	LSB 2
4	LSB 4
5	LSB 8
6	LSB 16
7	Execute

Appendix C

Instrument Calibration Table

j	Measurement	Scale Factor	Offset
1	VSA	15240.9 mGals/Hz	4330.71 Hz
2	OVEN TEMP.	10.0 DEG C/VOLT	20.0 DEG C
3	MAGNETIC COMPASS	5 VOLTS/360 DEGREES	
4	BOX TEMP.	10.0 " " "	20.0 " "
5	X GYRO (LOW)	0.4225 DEG/SEC/VOLT.	-1.095 DEG/SEC
6	Y GYRO (LOW)	0.4464 " " "	-1.126 DEG/SEC
7	Z GYRO (LOW)	-0.4375 " " "	1.103 " "
8	X GYRO (HIGH)	0.04367 " " "	-0.1443 " "
9	Y GYRO (HIGH)	0.04464 " " "	-0.1143 " "
10	Z GYRO (HIGH)	-0.08997 " " "	0.2352 " "
11	X ACCL (LOW)	-1.948 M/SEC**2/VOLT	4.882 M/SEC**2
12	Y ACCL (LOW)	-1.954 " " "	4.893 " "
13	Z ACCL (LOW)	1.995 " " "	4.918 " "
14	X ACCL (HIGH)	-0.07787 " " "	0.1954 " "
15	Y ACCL (HIGH)	-0.07815 " " "	0.1999 " "
16	Z ACCL (HIGH)	0.07838 " " "	9.608 " "
17	X MAG.	-238.9 MILLIGAUS/VOLT	-597.8 MILLIGAUS
18	Y MAG.	-239.7 " "	-599.3 "
19	Z Mag.	239.2 " "	-598.5 "